Synthesis and Characterization of Graphite Oxide Derived TiO_2-Carbon Composites as Potential Electrocatalyst Supports

Topics in Catalysis (2021)

Ilgar Ayyubov, Irina Borbáth, Zoltán Pászti, Zoltán Sebestyén, Judith Mihály, Tamás Szabó, Erzsébet Illés, Attila Domján, Mihaela Florea, Dana Radu, Andrei Kuncser, András Tompos, Emília Tálas

DOI: https://doi.org/10.1007/s11244-021-01513-1

Source Type: Journal

Original language: English

Document Type: Original Paper

Publisher: Springer Nature

Corresponding authors: Mihaela Florea, Emília Tálas

Accepted: 23 September 2021

Published: 05 October 2021

Synthesis and characterization of graphite oxide derived TiO_2-carbon composites as potential electrocatalyst supports

Ilgar Ayyubov[1], Irina Borbáth[1], Zoltán Pászti[1], Zoltán Sebestyén[1], Judith Mihály[1], Tamás Szabó[2], Erzsébet Illés[3], Attila Domján[4], Mihaela Florea[5], Dana Radu[5], Andrei Kuncser[5], András Tompos[1], Emília Tálas[1]

[1]*Research Centre for Natural Sciences, Institute of Materials and Environmental Chemistry, Eötvös Loránd Research Network (ELKH), Magyar Tudósok körútja 2, H-1117 Budapest, Hungary*

[2]*Department of Physical Chemistry and Materials Science, University of Szeged, H-6720 Szeged, Rerrich Béla tér 1, Hungary*

[3]*University of Szeged, Faculty of Engineering, Department of Food Engineering, H-6724 Szeged, Mars tér 7, Hungary*

[4]*Research Centre for Natural Sciences, Centre for Structural Science, Eötvös Loránd Research Network (ELKH), Magyar Tudósok körútja 2, H-1117 Budapest, Hungary*

[5]*National Institute of Materials Physics, 405A Atomistilor Street, 077125, Magurele, Romania*

Acknowledgement

The research within project No. VEKOP-2.3.2-16-2017-00013 was supported by the European Union and the State of Hungary, co-financed by the European Regional Development Fund. Project No. NNE130004 has been implemented with the support provided from the National Research, Development and Innovation Fund of Hungary, financed under the TR-NN-17 funding scheme. Project No. NNE 131270 has been implemented with the support provided from the National Research, Development and Innovation Fund of Hungary financed under the M-ERA.NET-2018 funding scheme. The financial supports by the János Bolyai Research Scholarship of the Hungarian Academy of Sciences are gratefully acknowledged (Erzsébet Illés). The authors also thank Dr. Ágnes Szegedi and Dr. Szilvia Klébert for the nitrogen physisorption measurements, and Dr. Zoltán May for the ICP-OES measurements.

*corresponding author, Tel.:+40721760041, email: mihaela.florea@chimie.unibuc.ro <mailto:mihaela.florea@chimie.unibuc.ro>, address: National Institute of Materials Physics, 405A Atomistilor Street, 077125, Magurele, Romania (Mihaela Florea)

Abstract:

TiO_2-C (carbon) hybrid materials are promising electrocatalyst supports because the presence of TiO_2 results in enhanced stability. Use of new types of carbonaceous materials such as reduced graphene oxide (rGO) instead of traditional active carbon provides certain benefits. Although the rutile polymorph of TiO_2 seems to have the most beneficial properties in these hybrid materials, the anatase type is more frequent in TiO_2-rGO composites, especially in graphite oxide (GO) derived ones, as GO has several properties which may interfere with rutile formation. To explore and evaluate these peculiarities and their influence on the composite formation, we compared TiO_2-C systems formulated with GO and Black Pearls (BP) carbon. Various physicochemical methods, such as attenuated total reflection infrared (ATR-IR)-, solid state NMR-, Raman- and X-ray photoelectron spectroscopy, X-ray powder diffraction (XRD), electron microscopy, etc. were used to characterize the samples from the different stages of our multistep sol-gel synthesis. Our experiments demonstrated that utilization of GO is indeed feasible for composite preparation, although its sodium contamination has to be removed during the synthesis. On the other hand, high temperature treatment and/or solvothermal treatment during composite synthesis resulted in decomposition of the functional groups of the GO and the functional properties of the final product were similar in case of both composites. However, Pt/TiO_2-GO derived sample showed higher oxygen reduction reaction (ORR) activity than Pt/TiO_2-BP derived one. Based on the decrease of electrochemical surface area, the stability order was the following: Pt/C (commercial) < Pt/TiO_2-BP derived C < Pt/TiO_2-GO derived C.

Keywords: graphite oxide, reduced graphene oxide, composite material, solvothermal treatment, Pt electrocatalyst

1. Introduction

TiO_2-C hybrid systems have already attracted considerable interest as, photoelectrocatalysts [1,2] electrocatalysts [3] and electrocatalyst supports [4-8]. Enhanced electrochemical performance in the reactions usually catalyzed by oxophilic metals, as well as improved stability of TiO_2-C composite supported Pt electrocatalysts, has been described [6,9,10].

Great variety of methods producing TiO_2-C hybrid systems can be found in the literature depending on the goals of the different studies; some examples are given below. In references [4,8,11] pre-prepared TiO_2 was surrounded by carbon derived from high temperature carbonization of the carbon source. Another approach utilizing pre-prepared TiO_2 is its connection to the carbonaceous material by use of hydrothermal /solvothermal treatment [12]. A different class of preparation techniques involve direct hydrothermal/solvothermal synthesis from various Ti- precursors such as $Ti(SO_4)_2$ [13], tetrabutyl orthotitanate [2], titanium (IV) n-butoxide [1], $(NH_4)_2TiF_6$ [14] in the presence of carbonaceous material or hydrolysis of Ti precursor in the presence of carbonaceous material [15,16]. Sol-gel method from titanium tetraisopropoxide in the presence of a carbon source followed by thermal treatment is also a feasible way [17]. As a result of the different synthesis approaches, great variety of both the TiO_2 and the carbonaceous phases in these hybrid materials can be found; high temperature carbonization most likely leads to rutile TiO_2 phase [11], while hydrothermal synthesis results in anatase [1,2,12]. In certain cases, TiO_2 can also be kept in amorphous phase [15].

Regarding the carbonaceous part, beside pre-prepared and *in situ* formed activated carbon, new types of carbonaceous materials such as reduced graphene oxides (rGO) are increasingly used in TiO_2-C hybrid materials. Graphene derivatives provide special properties, including increased electrical and thermal conductivity, chemical and mechanical stability to inorganic oxide-carbon composites [18]. Exfoliated graphite oxide (GO) offers several advantages as carbonaceous starting material for composites; this novel material with abundant oxygen containing functional groups is relatively cheap and suitable for mass production. The GO is weakly acidic material in aqueous dispersions [19] due to its dissociable functional groups which are covalently attached to the carbon skeleton [20,21]. As a result, GO has a highly hydrophilic character compared to the parent graphite which makes its handling easier during the composite preparation unlike the hydrophobic graphene [22]. GO can be easily transformed to rGO which leads to formation of a graphene like units in the composite. Synthesis and characterization of GO derived TiO_2-carbonaceous material composites for photocatalytic purposes have been widely studied [22-26]. A large number of studies reported

also about the successful use of GO in TiO_2-C (C: carbonaceous material) and noble metal/TiO_2-C composites in various fields of electrocatalysis such as N_2 reduction reaction [27], methanol oxidation [7,13,28] or oxygen reduction reaction (ORR) [12,14,17,29]. Combination of rGO with other layered inorganic materials is also useful tool; e.g. it can help to overcome the difficulties caused by the poor conductivity of layered double hydroxides (LDHs) in applications for oxygen evolution reaction (OER) [30]. An entirely different class of 2D materials is obtained if the hybrid-forming approach is taken to the extreme limit of mixing on the atomic scale: the resulting MXenes, involving Ti-carbide-based systems, seem to be interesting novel systems either as electrocatalysts themselves or as electrocatalyst supports [31,32].

In our previous studies we proposed novel, TiO_2 based mixed oxide-carbon composite supported platinum electrocatalysts (Pt/$Ti_{(1-x)}Mo_xO_2$-C) for polymer electrolyte membrane fuel cells (PEMFCs). Above catalysts showed better stability and increased CO tolerance compared to the state-of-the-art PtRu/C ones [33,34]. We have developed a multistep sol-gel-based synthesis method for these supports in which first TiO_2-rutile nuclei are grown on the carbon backbone at low temperature, completed by an aging step, then the Mo precursor is added and incorporated into the TiO_2-rutile crystallites during a high-temperature treatment (HTT) step [33-36]. In this method the presence of rutile nuclei before HTT is an important prerequisite of the dopant incorporation into the mixed oxide phase [37].

Taking into account the proven performance of the GO-based systems in many catalytic applications and the promising behavior of the transition metal doped TiO_2-C composites as electrocatalyst supports, it is tempting to consider the suitability of GO for use in TiO_2-C type composites containing the rutile TiO_2 phase. Indeed, it is widely believed that functional groups of the carbon backbone can anchor the oxide particles [38-40] and/or the Pt particles [41], resulting in catalysts with enhanced stability. In this sense it can be assumed that GO represents the extreme case of functionalized carbon materials for anchoring oxides [42,43] and metals [44-46]. Accordingly, the aim of the present work is to adapt our previously developed multistep sol-gel method for the preparation of rutile TiO_2-GO derived C composites. Rutile phase is regarded more thermodynamically stable than other polymorphs of TiO_2 [47,48]. Moreover, recent research suggests high potential of rutile TiO_2 as a support material for electrocatalysts [49]. Nevertheless, two characteristic properties of GO have to be taken into account when considering the possibility of adapting GO to our previously developed composite preparation method.

The first one concerns the disintegration of the parallel stacked, multilayered assemblies of GO, *i.e*. delamination or exfoliation of the GO, which is assumed to play a key role in having the appropriate specific surface area of the composite. Different methods, such as sonication, thermal treatment, microwave treatment, etc. can be used for the exfoliation of GO [22]. As the negative charge developed on the functional groups of the GO layers in basic medium generates a repelling interaction, slightly basic conditions can also help to achieve larger degrees of dispersion [19]. However, strong acidic medium adjusted by HNO_3 is necessary for the formation of the rutile phase TiO_2 nuclei. A possible workaround is making a slurry of GO sonicated in a slightly alkaline medium and its vigorous mixing with the acidic colloidal TiO_2 precursor solution under strict pH control, as done in our previous attempt, which resulted in successful composite preparation [36]. This composite had a specific surface area of more than 100 m^2/g and the Mo incorporated mainly into the $Ti_{(1-x)}Mo_xO_2$ mixed oxide part of rutile type after the HTT [36]. However, there are several peculiarities of this approach which were not revealed yet, and GO derived TiO_2-C systems seems to be good model system for this purpose.

The other property of the GO which has to be taken into account is its heat sensitivity. This issue needs to be addressed because a HTT step cannot be avoided for the formation of rutile phase of TiO_2. It is known that GO is thermally unstable; it decomposes slowly at relatively low temperatures (60-70°C) with formation of CO, CO_2, H_2O and turbostratic carbon. Thermal instability of GO can be associated with the exothermic decomposition reactions of oxygen-containing groups in the basal plane and periphery of graphite layers [50]. The decomposition of GO under very slow heating can be regulated but an increased heating rate results in thermal explosion [50]. Latter phenomenon is also called as deflagration. During deflagration great amount of formed gaseous products lead to the delamination of GO particles, a sudden decrease in the oxygen content of the material, and the formation of a certain type of turbostratic carbon, a graphene-like substance with rather high specific surface area [51]. It has been also described that the oxygen-containing groups of GO are generally decomposed in three temperature regions of 170–250, 500–600, and 750–1000 °C [50]. The above carbonaceous materials of large specific surface area appear to meet the requirements of the electrocatalyst support. However, it is an open question whether this type of carbonaceous material provides extra advantages to the composite support and the Pt electrocatalyst supported on it in comparison with the composite obtained from an ordinary carbon material.

Since the main motivation behind development of oxide-carbon composite supports is to enhance the stability of the resulting catalysts, ensuring intimate contact between the oxide and the carbon is a key requirement. According to the literature, electrostatic interactions

between the graphitic carbon material and the metal oxide in the TiO_2-GO systems can be important in this sense [25,52] but chemical bond formation between Ti-OH and functional groups of GO is also suggested [7]. Solvothermal or hydrothermal procedure used in order to connect TiO_2 nanoparticles to GO sheet [53-55], results in rGO with parallel removal of the O-containing functional groups of GO [7]. This process leads to re-establishment of conjugated graphene network [56] and to the possible appearance of C-O-Ti bonds [7,54,57,58].

According to the above considerations, prior to application of GO as a source for the carbonaceous material in TiO_2-C composite electrocatalyst supports, a few questions has to be clarified. One of them is the mitigation of the apparent conflict between the highly acidic milieu needed for exclusive TiO_2-rutile deposition and the mildly basic environment preferred for GO delamination. The other is the relevance of the functional groups for rutile growth in the initial stage of the composite preparation and the effect of their partial or complete elimination upon high temperature treatment.

The aim of the present work is to provide insight into these carbonaceous phase related issues by comparing the structural and functional properties of TiO_2-C composites prepared by multistep sol-gel method on GO-derived and carbon black materials. Our further aim is to achieve the exclusive formation of the rutile TiO_2 phase in these composites, as the ultimate goal in our future work is to use these knowledge to prepare various metal (W, Mo, Sn, Nb) doped TiO_2-GO derived carbon composites as potential catalyst supports for Pt electrocatalysts in PEMFCs. Apart from physico-chemical characterization of the graphite oxide-derived TiO_2-C composites, their effect on the electrocatalytic properties of platinum catalyst supported on them are also studied and compared to those of carbon black derived ones.

2. Experimental

2.1. Materials

NaOH was purchased from Reanal. HNO_3 (65%, a.r.) and 2-propanol were products of Molar Chemicals. Titanium-isopropoxide (Ti(O-*i*-*Pr*)$_4$, Aldrich, 97%) was used as Ti precursor compound. Black Pearls 2000 (BP) supplied by Cabot and graphite oxide (GO) were used as carbon materials. GO was prepared from graphite by the Hummers-Offeman method. GO (I) suspension (3.2 wt.% for carbon) was purified by dialysis while GO (II) suspension (0.95 wt.% for carbon) was used without purification. Hexachloroplatinic acid hexahydrate ($H_2PtCl_6 \times 6H_2O$, 37.5 % Pt, Sigma-Aldrich) was used as Pt precursor compound.

2.2. Preparation of composites and composite supported catalysts

Figure 1 demonstrates the flow-charts for preparing mixed oxide-GO derived carbonaceous material composite supports by using sol–gel-based multistep synthesis routes.

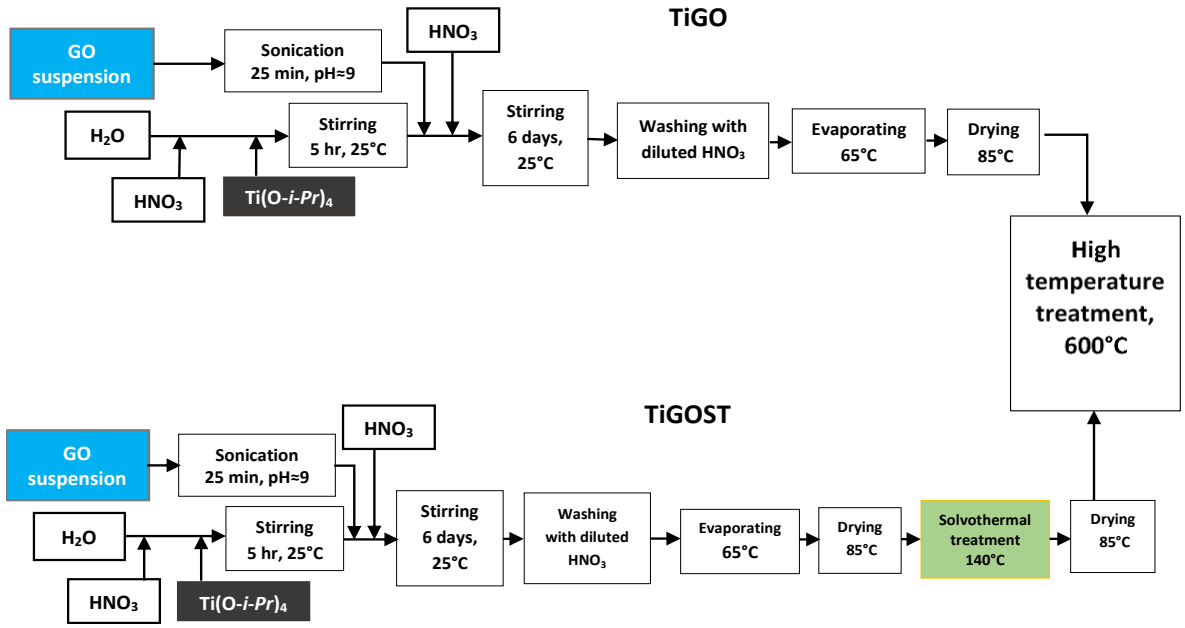

Fig. 1 Flow charts for preparing TiO_2-GO derived carbonaceous material composite supports by using sol–gel-based multistep synthesis routes

Typically, a transparent acidic TiO_2 colloidal solution was made first by adding Ti(O-*i*-*Pr*)$_4$ into the vigorously stirred mixture of cc. HNO_3 and distilled water as described in the Supplementary Materials. The suspension with the desired amount of GO was weighted. The exfoliation of GO by use of NaOH, the mixing of the TiO_2 colloidal solution with the exfoliated GO suspension, its pH control and the aging step were carried out as we described before (see Ref. [36] and Supplementary Materials). .$NaNO_3$, formed as a byproduct of the procedure, was removed by washing in HNO_3. The samples obtained in the drying step at 85 °C were visually homogeneous; no phase separation could be observed.

In case of the solvothermal treatment (ST) step, the solid sample dried at 85 °C was sonicated in 100 mL 2-propanol for a short time (5-10 min) then the slurry was placed into a glass lined autoclave. After rinsing with nitrogen the temperature inside was increased to 140-150 °C in ~1-1.5 h and it was kept at this temperature for ~3 h on autogenic pressure. The reaction mixture was then allowed to cool, centrifuged, air-dried at RT and dried again in an oven at 85 °C overnight.

As a final step of the synthesis of the catalyst support material, a high temperature treatment (HTT) for 8 h at 600 °C in Ar atmosphere was performed to get well crystallized rutile TiO_2.

For comparison, BP derived TiO_2-C samples were also prepared according to the above procedure but the second HNO_3 addition step for pH setting and washing with HNO_3 was omitted.

Table 1 summarizes the nominal compositions and preparation details of the various TiO_2-C composites till the stage before HTT. Denominations of the samples from the different phases of the preparation are the following: the name used in Table 1 means composite support materials after drying at 85° C; ST indicates solvothermally treated sample; HT indicates high temperature heat treated sample, while Cat means the catalyst samples obtained with loading of 20 wt.% Pt on the high temperature treated composite.

Table 1. Preparation details of TiO_2-C (C= BP and GO derived carbonaceous material) composites till the stage before HTT. Nominal composition: 75 wt.% TiO_2-25 wt.% C.

No	Type of C	TiO_2 sol			Added suspension of the carbonaceous material		$NaNO_3$ removal (washing step)	ST[c]
		H_2O, ml	HNO_3[a], ml	Ti prec., ml[b]	C, g	H_2O, ml		
TiGO-1	GO(I)	29	1.52	1.079	0.17[d] (in 5.25 g)	10	no	no
TiGO-1ST	GO(I)	29	1.52	1.079	0.17[d] (in 5.25 g)	10	no	yes
TiGO-2	GO (II)	29	1.52	1.079	0.17[d] (in 17.78 g)	-	no	no
TiGO-3	GO (II)	29	1.52	0.79	0.17[d] (in 17.78 g)	-	yes	no
TiBP	BP	21	2.35	2.05	0.25	10	no	no

[a] cc. HNO_3 (65%, Molar Chemicals, a.r.);
[b] Ti precursor compound: $Ti(O\text{-}i\text{-}Pr)_4$;
[c] ST: solvothermal treatment before HTT in 2-propanol at 140°C;
[d] pH adjusted to 9 with concentrated NaOH solution.

The TiO_2-C support materials were loaded with 20 wt.% Pt via a modified, sodium borohydride ($NaBH_4$) assisted ethylene-glycol (EG) reduction-precipitation method (see Figure S1 in the Supplementary Materials) in order to obtain platinum containing electrocatalyst as we described before [33].

2.3. Physicochemical characterization

X-ray powder diffraction (XRD), nitrogen physisorption measurements, X-ray photoelectron spectroscopy (XPS) measurements were carried out using the same equipment and methods as in our previous studies [36] (see in Supplementary Materials).

Transmission electron microscopic images were taken by a Philips CM-10 and a JEOL-3010 transmission electron microscope with an accelerating voltage of 100 kV and 300 kV, respectively (see also in the Supplementary Materials).

Scanning electron micrographs of the samples were recorded with a scanning electron microscope Vega II LMU model from Tescan, equipped with an energy dispersive X-ray spectrometer (EDX) Bruker Quantax 200 (see details in the Supplementary Materials).

Raman spectra were obtained on a LabRAM HR Evolution spectrometer from Horiba Jobin Ivon, with a laser radiation at wavelength of 633 nm. All spectra were recorded at room temperature in the extended scan mode in the 50 and 2000 cm^{-1} range.

ATR-IR spectra were recorded by the means of a Varian 2000 (Scimitar Series) FT-IR spectrometer (see details in the Supplementary Materials).

Solid state NMR magic angle spinning (MAS) spectra of samples were recorded on Varian System spectrometer with a Chemagnetics 3.2 mm narrow-bore triple resonance T3 probe in double resonance mode (see details in the Supplementary Materials)..

Thermogravimetric (TG) measurement was carried out with a PerkinElmer TGS-2 thermobalance in a compressed air atmosphere. The flow rate (volumetric flow) of the gas was 140 ml/min during the test. Approx. 1 mg sample was weighed. The TG furnace heat program has heated the sample from room temperature (1-minute running time) to 900 °C at a heating speed of 5 °C/min

The Pt content of the samples was measured by inductively coupled plasma-optical emission spectrometry (ICP-OES) technique by use of a simultaneous SPECTRO GENESIS instrument with axial plasma observation. Samples were measured after microwave assisted dissolution in 1:2:6 mixtures of concentrated hydrofluoric acid: hydrochloric acid: nitric acid.

2.4. Electrochemical characterization

The details of the electrochemical characterization including the preparation of working electrode, the composition of catalyst ink and electrocatalytic measurements were described in Refs. [33,36,59] and Supplementary Materials. The measurements were done in a standard three-electrode cell using 0.5 M H_2SO_4 electrolyte solution. The Pt loading of the electrodes was 10 µg cm^{-2}. Glassy carbon (surface area: 0.0707 cm^2) was used as working electrode, platinum wire as counter electrode and a hydrogen electrode as reference electrode. All potentials are given on RHE scale.

Electrocatalytic performance of the 20 wt.% Pt/TiO_2-C electrocatalysts was studied by cyclic voltammetry, CO_{ads}-stripping voltammetry and ORR measurements done before and

after the 500-cycle stability test, as well as by the long-term stability test involving 10,000 polarization cycles (for details see Supplementary Materials).

Electrochemically active Pt surface area ($ECSA_{Hupd}$) was determined from the charge needed for oxidation of underpotentially deposited hydrogen on the platinum surface according to the traditional method (Ref. [60], Equation S1, Supplementary Materials). The stability of the catalysts was assessed by following the change of the ECSA during polarization cycles between 0.05 and 1.00 V potential limits (Equation S2, Supplementary Materials).

ORR activity of the catalyst samples in O_2 saturated 0.5 M H_2SO_4 solution was tested by rotating disc electrode (RDE) technique (for details see Ref. [61] and Supplementary Materials).

3. Results and discussion

3.1. Effect of the high temperature heat treatment (HTT)

Our previous experience with carbon black based composites showed that HTT is essential for the formation of the rutile type of mixed oxide phase [33]. Thermal instability of pure GO was also well-known [50], however we had no information about an important issue, how the GO derived carbonaceous part in the composite changes during the HTT. It was also known from the literature that the GO served as binding site for Ti species during the hydrolysis of the Ti-precursor [62], but we had no information how this type of close contact between TiO_2 and GO in the composite influences the thermal stability of the GO derived part. Removal of the functional groups of and formation of Ti-C bond during hydrothermal/solvothermal treatments [54] led us to the assumption that an rGO-like carbon material obtained by ST at about 150 °C would be relatively stable during HTT. Regarding the conditions of ST, it is worth mentioning that 2-propanol is known as agent for catalytic transfer hydrogenations [63].

Portions of sample TiGO-1 dried at 85 °C were treated in Ar at different temperatures (150 °C, 300 °C, 600 °C) for 8 h then characterized by ATR-IR spectroscopy and ^{13}C solid state NMR. Selected samples were studied by TEM and XRD too.

According to results of ATR-IR spectroscopic measurements signals of oxygen-bearing groups (carbonyl vibration at 1711 cm^{-1}, carboxyl group vibrations at 1623, 1406, 1328 cm^{-1} and C-O-C and C-O-H stretching bands of ether and/or alcoholic groups around 1059 cm^{-1}) appeared in the spectrum of the untreated sample (line **a** in Figure 2A). The band around 1623 cm^{-1} can be assigned to C=C bonds, too. This spectrum was very similar to that reported by Majrik *et al*. for 10 % GO/TiO_2 sample prepared by heterocoagulation method [26]. Upon heating the sample TiGO-1 at 150 °C in Ar the characteristic features of the spectrum did not

change (line **b** in Figure 2A). After the treatment of sample TiGO-1 at 300 °C the vibrational bands characteristic for carboxyl groups and/or C=C double bond (1623, 1406 and 1328 cm^{-1}) disappeared while a broad band attributed to surface carbonate/hydrocarbonate (1559 cm^{-1}) appeared indicating the significant changes of the sample (line **c** in Figure 2A).

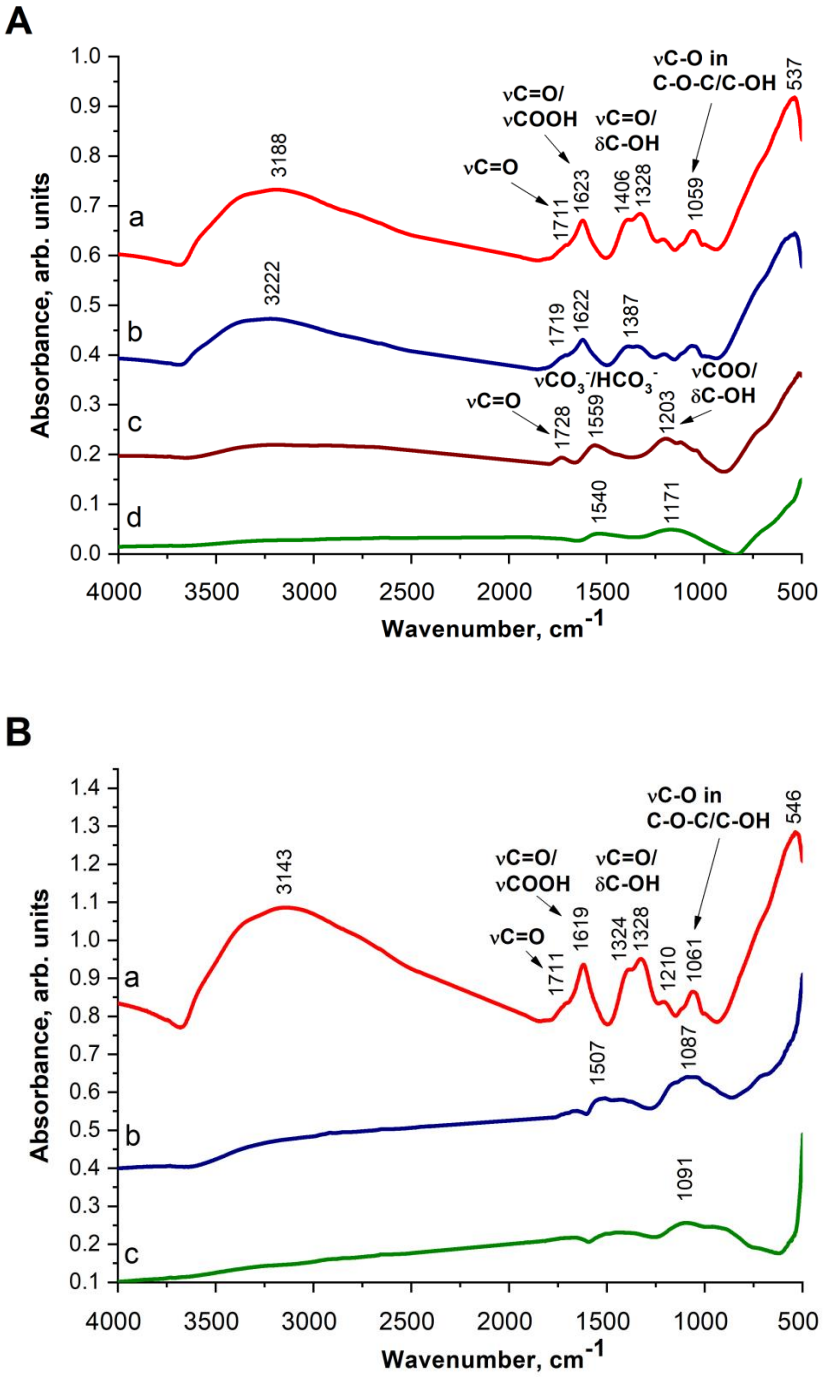

Fig. 2 ATR-IR spectra of TiGO-1 derived samples after various treatments. **(A)** annealing of TiGO-1 without solvothermal treatment. **a**: TiGO-1 without annealing, **b**: annealing at 150 °C in Ar, **c**: annealing at 300 °C in Ar, **d**: after HTT at 600 °C (TiGO-1HT).
(B) annealing of TiGO-1 after ST. **a:** TiGO-1 (from parallel preparation), **b**: TiGO-1ST, **c**: solvothermally treated TiGO-1ST after HTT at 600 °C (TiGO-1STHT).

Further increase in the temperature of the treatment resulted in a featureless spectrum due to the significant change in the structure of the carbonaceous part with the loss of the functional groups (line **d** in Figure 2A). It has to be noted, however, that the background correction was problematic because this sample was too black.

^{13}C solid state NMR spectra of TiO_2-GO derived samples can be seen in Figure 3. Line **a** in Figure 3A confirmed the ATR-IR results *i.e.* the untreated sample had several types of functional groups (carbonyl, C-OH, O-C-O) and sp^2 hybridized carbon. NMR results indicated the presence of certain aliphatic carbon, too. As a result of the heat treatment in Ar at 600 °C (line **b** in Figure 3A) the intensity of the signals decreased except of that of the phenolic OH and the sp^2 hybridized carbon which indicated again the removal of the functional groups under the HTT. However, we could not get information about a possible rupture of the GO sheets under the HTT by means of these methods.

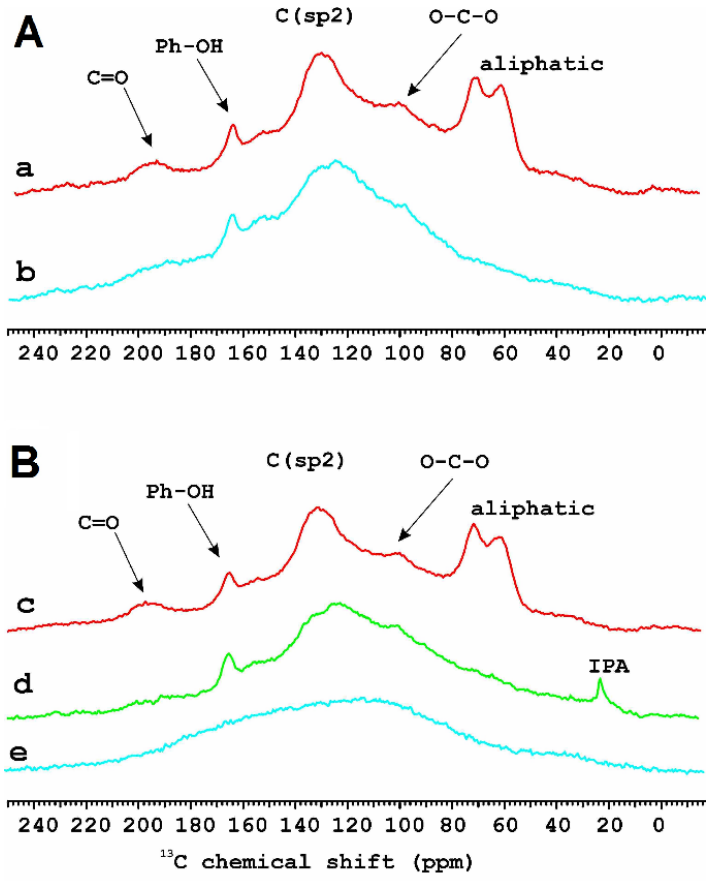

Fig. 3 ^{13}C solid state NMR spectra of TiGO-1 derived samples after various treatments. Panel A: without and panel B: with solvothermal treatment. **a**: TiGO-1 without treatment, **b**: TiGO-1 annealed at 600°C in Ar (TiGO1-HT), **c:** TiGO-1 from parallel preparation, **d**: TiGO-1 after solvothermal treatment (TiGO-1ST), **e**: solvothermally treated TiGO-1ST after HTT at 600 °C (TiGO-1STHT)

Figure 2B shows the comparison of samples prepared with and without ST prior to HTT by use of ATR-IR spectroscopy (Figure 2B). No well-defined bands related to functional groups can be detected in the IR spectrum of the sample after the ST at 150 °C (line **b** in Figure 2B). It is interesting that an almost "band-free spectrum" was obtained after annealing of the solvothermally treated sample (TiGO1-STHT, line **c** in Figure 2B).

Above results were consistent with those of ^{13}C NMR measurements. By ^{13}C NMR 2-propanol was also detected (line **d** in Figure 3B). It has been known that due to its layered structure and oxygen containing functional groups GO strongly intercalates H_2O between its layers [64]. Obviously, during the solvothermal treatment the intercalated water more or less could be exchanged to 2-propanol. Probably, we observed its remnants after drying at 85 °C. Decreased intensity of the carbon containing functional groups (except of phenolic OH) after the ST was in line with the picture developed in the literature [54].

The most important observation was that the ^{13}C NMR spectra of the different samples treated at 600 °C were different (*cf.* line **b** and **e** in Figure 3). After HTT the sample that underwent previous solvothermal treatment appeared to be completely graphitized. Presence of this highly graphitic carbon without functional groups suggested that the structure of the carbonaceous part was closer to the rGO structure in the TiGO-1STHT sample than it was in TiGO-1HT without ST.

Both ATR-IR and ^{13}C NMR measurements proved that the first stage of the composite production method resulted in a well-reproducible product regarding the carbonaceous part. TiGO-1 from parallel preparations resulted in very similar patterns by ATR-IR spectroscopy (*cf.* line **a** in Figure 2A and line **a** in Figure 2B) as well as by ^{13}C NMR spectroscopy (*cf.* line **a** and **c** in Figure 3).

The pictures showed by ATR-IR and ^{13}C NMR spectroscopy for the same sample were slightly different which could be explained by the fact that in case of ATR techniques the penetration depth into the sample is typically between 0.5 and 2 μm while magic angle spinning (MAS) technique in solid state NMR spectroscopy provides information about the whole bulk phase.

TEM images of composites obtained with and without solvothermal treatment after annealing at 600 °C in Ar confirmed the differences in the carbonaceous part (Figure 4).

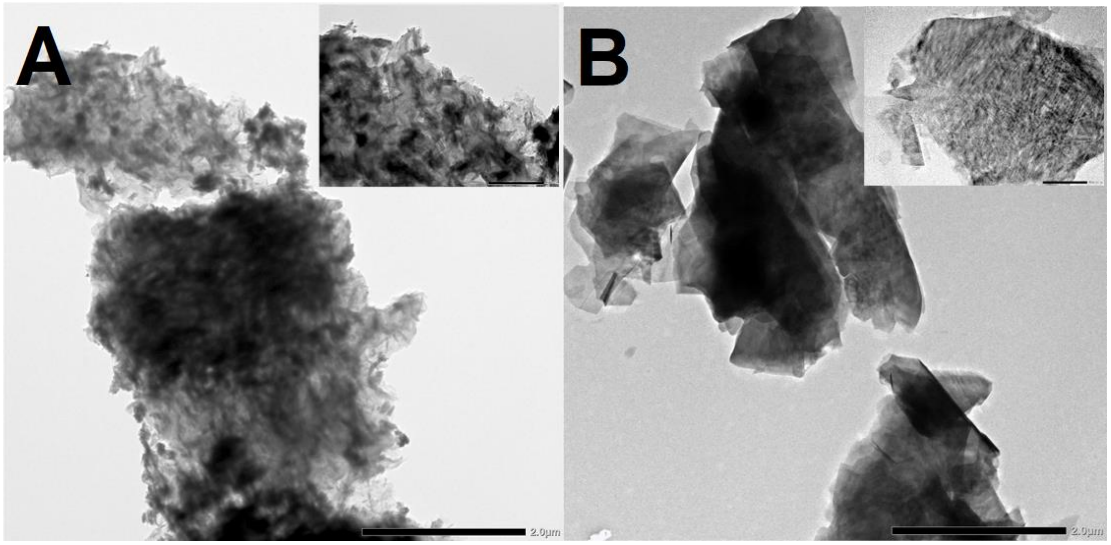

Fig. 4 TEM images of the TiGO-1 derived samples after various treatments.
A: TiGO-1HT; B: TiGO-1STHT. Bar: 2 μm (500 nm in the inserts).

Typical low resolution image of TiGO-1HT showed that particles of micrometer size formed as a result of heat treatment (Figure 4A). The "waviness" of the particles which were visible even under the middle darkest area was clearly corresponding to the presence of the r-GO. It is even better observable in the edges/around the edges (insert of Figure 4A). TiO_2 appeared mainly in the form of elongated, stick-shaped particles (Figure 4A). In addition, near the edges of the composite particle, the wrinkled (typical thermally degraded GO) carbon phase was well noticeable. The morphology of the carbon phase in case of solvothermally treated TiGO-1STHT sample (Figure 4B) differed significantly from that obtained without ST. The crystallinity of the carbon was improved, and the lamellae were less crumpled, and much more graphitic than without ST. However, much smaller amount of oxide particles seemed to be remained on the carbon lamellae, which could be consistent with the fact that the polarity of the carbon phase had been severely reduced and it might have lost most of the charge carrier groups.

SEM images (Figure S2 in the Supplementary Materials) confirm the different morphology of the samples prepared with and without ST step prior to HTT.

XPS investigation of composites prepared on GO confirms the above results. In Figure 5 C 1s spectra of TiGO-3HT is compared to those of a pristine GO sample and TiBPHT, a composite prepared on BP carbon material. In particular, the spectrum of the untreated GO is in good agreement with the IR and NMR results: the carbonaceous backbone which is represented by a broad graphite-like feature (peak around 284.4 eV) carries a high amount of functional groups, containing mainly C-O bonds (C-OH or C-O-C groups, contributing to the peak around 286 eV) along with a considerable amount of carbonyl-like species (around 287-

288 eV) [65]. A smaller peak around 285 eV can arise from aliphatic groups as indicated already by the NMR measurement.

On the other hand, the C 1s spectrum of the GO-based composite is almost identical to that of graphitic carbon. The line shape of the contribution arising from C-C bonds was measured on graphitic carbon and analysis of the spectrum of the GO-based composite indicated only a small additional C-O-like contribution. Therefore, the XPS measurement also confirmed the elimination of functional groups during composite formation and high temperature treatment. In fact, according to the XPS results, the carbonaceous material in the GO derived composite seems to be very similar to that in the BP based material.

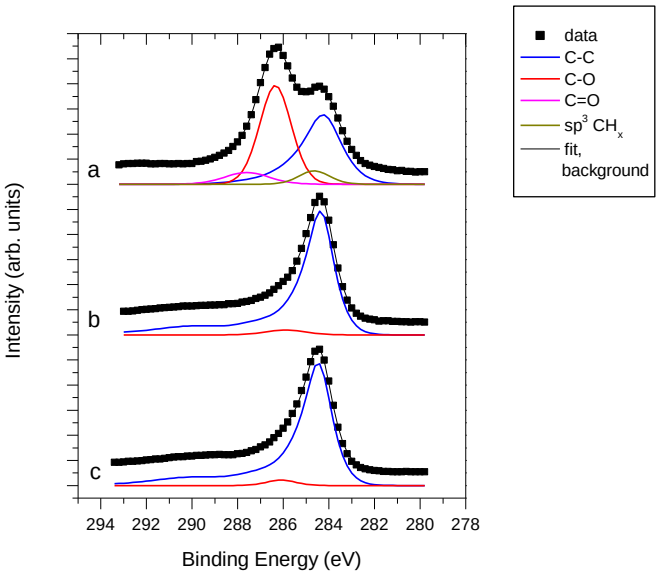

Fig. 5 C 1s spectra of a: pristine GO, b: TiO_2-GO derived carbon composite after high temperature treatment (TiGO-3HT) and c: TiO_2-Black Pearls composite after high temperature treatment (TiBPHT).

The XPS measurement confirmed the presence of TiO_2 in both the GO derived and the BP-based composites. However, quantitative evaluation revealed only 36 wt.% oxide in the GO derived sample and 43 wt.% in the BP-based composite, instead of the nominal 75 wt.%. In our previous work with Mo containing composites a general observation was that XPS detected more carbon than the nominal carbon content; the mixed oxide/C weight ratio was about 60/40 in case of a nominally 75 wt.% mixed oxide / 25 wt.% BP material [36]. The apparent conflict between the XPS results and the nominal composition suggests that the assumption behind the quantitative XPS analysis (i.e. the homogeneous distribution of the components within the sampling depth of the method) is not valid. Indeed, if, in addition to more dispersed forms, the oxide phase contains also larger crystallites with thickness above the sampling depth (around

10 nm), the surface specific XPS technique underestimates the oxide content [36]. The apparent oxide content of the TiO_2-C composites observed here is even smaller than that of a typical $Ti_{0.8}Mo_{0.2}O_2$-C composite, which suggests that the oxide forms relatively large crystallites with incomplete coverage on the carbon backbone, regardless to the source of the carbon. Although this result is in agreement with the TEM results of Figure 4, it also means that the decomposition of the functional groups during the high temperature treatment eliminates their anchoring effect in stabilizing the dispersion of the oxide.

3.2 Formation and removal of $NaNO_3$ during composite synthesis

Our previous works indicated that strong acidic media adjusted by HNO_3 was necessary for the formation of the TiO_2-rutile nuclei [36]; while media of much higher pHs (added NaOH) was useful for the delamination of GO [19]. Our working hypothesis was that addition of 5 hours aged solution of Ti(O-*i*-*Pr*)$_4$ to delaminated GO under vigorous stirring results in exclusively rutile phase of TiO_2 after the HTT. However, formation of $NaNO_3$ was unavoidable during this procedure. Based on the literature we came to the conclusion that the presence of $NaNO_3$ during the HTT is harmful, because it decomposes thermally above 450 °C with oxygen formation (Equation 1) [66] leading to uncontrolled treatment conditions during the preparation; the released oxygen might burn a part of the carbonaceous material in the composite. The decomposition of $NaNO_2$ under the further heating results in Na_2O (Equation 2) [67], which can react further, but the presence of any Na compounds is supposed to be unfavorable for utilization of the aimed TiO_2-C composite as an electrocatalyst support.

$$2NaNO_3 \rightarrow 2NaNO_2 + O_2 \qquad \text{(Equation 1)}$$

$$2NaNO_2 \rightarrow Na_2O + NO + NO_2 \qquad \text{(Equation 2)}$$

It has to be mentioned that $NaNO_3$ can be present in the GO starting material, too, as the Hummers-Offeman method uses $KMnO_4$, H_2SO_4 and $NaNO_3$ for oxidation of graphite. GO can be purified from $NaNO_3$ by dialysis however this procedure is rather time consuming, furthermore it makes the preparation of the starting material expensive. We used both cleaned (GO(I)) and uncleaned (GO(II)) starting material in our experiments.

The results of XRD measurements of composites dried at 85 °C (Figure 6A) showed that the amount of crystallized $NaNO_3$ was significant only in sample TiGO-2 obtained by use of the unpurified GO (II) suspension starting material. In case of sample TiGO-3 prepared from GO (II) an additional washing step was inserted in order to remove the $NaNO_3$ (see Figure 1). This step was not used in our previous work when the carbonaceous part of the composite was

derived from BP carbon [33]. As it can be seen in Figure 6A, $NaNO_3$ was successfully removed by this washing procedure.

According to XRD results, samples TiGO-1HT, TiGO-2HT and TiGO-3HT which were obtained from TiGO-1, TiGO-2 and TiGO-3 by HTT contained only rutile TiO_2 phase (see Figure 6B). The characteristic signal for $NaNO_3$ at about 29° disappeared which was an indication of the thermal decomposition of $NaNO_3$.

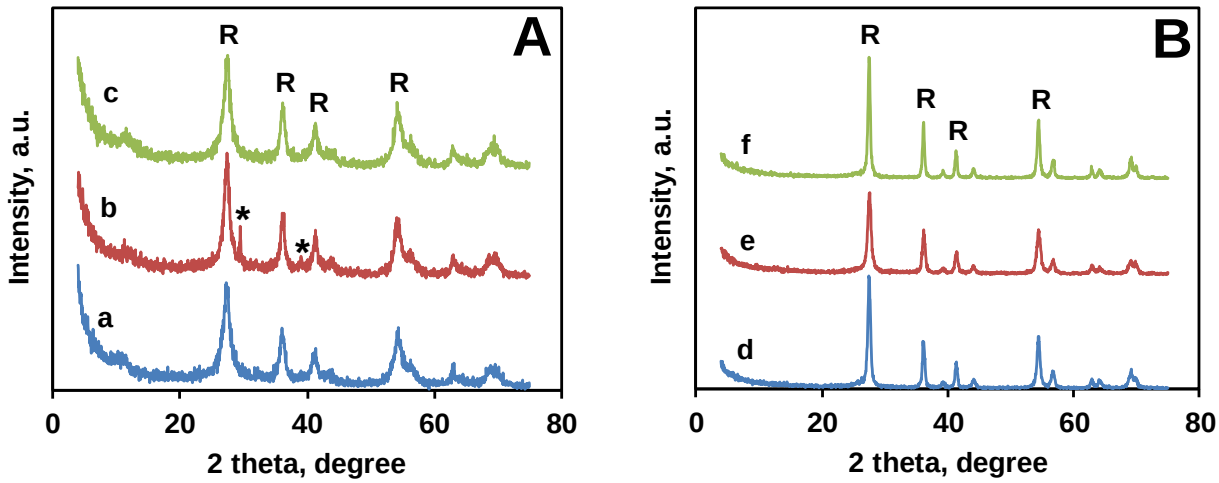

Fig. 6 XRD pattern of GO derived composites before (A) and after (B) HTT. **a**: TiGO-1, **b**: TiGO-2, **c**: TiGO-3, **d**: TiGO-1HT, **e**: TiGO-2HT, **f**: TiGO-3HT. R- rutile, *-$NaNO_3$ (R-3c, JCPDS, No. 71-1558)

Almost exclusive formation of rutile type of TiO_2 after drying (Figure 6A) and after HTT (Figure 6B) also indicated that this preparation method can be effective for dopant (e.g., W, Mo, Sn or Nb) incorporation into the oxide part of the composite in our further work. In line with XRD results, TEM images of all the high temperature treated samples showed elongated and thin agglomerates (see Figure S3 in the Supplementary Materials) most probably due to the presence of TiO_2-rutile. According to SEM images, the morphology of the above high temperature treated samples hardly differed (Figure S4 in the Supplementary Materials).

The effect of the presence of $NaNO_3$ during HTT was also indicated by TG measurements. The TG and DTG curves of samples TiGO-1HT, TiGO-2HT and TiGO-3HT derived from GO were rather similar to each other, but the TiBPHT material derived from BP carbon differed slightly (Figure S5 in the Supplementary Materials). The most important features of the thermal behavior of above samples are collected in Table 2.

Table 2. Thermal features of TiO_2-carbonaceous material composites

Sample	Origin of carbonaceous part	$NaNO_3$ removal	$T_{DTG\ max}$, °C	Ash content at 900 °C, %	Carbonaceous part, %
TiGO-1HT	GO(I)	-	465	82.92	17.08
TiGO-2HT	GO(II)	-	400	83.71	16.29
TiGO-3HT	GO(II)	+	475	79.21	20.79
TiBPHT	BP	n.r.	555	77.35	22.65

GO (I): graphite oxide with special purification, GO (II): graphite oxide without special purification, BP: Black Pearls (Cabot), n.r.: not relevant.

The ash content means the remaining material obtained after heating the samples up to 900 °C in air. The mass loss was related to the burning of the carbonaceous part. The ash content in each sample was somewhat higher than 75 % which was expected from the nominal 75/25 ratio. The difference was the smallest in case of the BP derived sample. The ash content of the unwashed samples was 3-5 % higher than that of washed one (*cf.* TiGO-1HT and TiGO-2HT to TiGO-3HT in Table 2). This difference could be attributed to the fact that some of the carbon material was really burned due to O_2 evolution from $NaNO_3$ during HTT step of the composite preparation and/or the Na-containing residue increased the ash content. Comparing the ash content of sample TiGO-3HT and TiBPHT only a slight difference could be found. Perhaps the real C/H/O ratio of the GO was slightly different from that we used for the calculations of the recipe and/or the samples may have contained O and H functional groups even after HTT. The mass loss of these samples occurred in one step (see Figure S5 in the Supplementary Materials). It is clearly visible from the data that the combustion of carbon material appeared at lower temperatures in case of GO than in case of BP (see $T_{DTG\ max}$ in Table 2). Furthermore, the presence of $NaNO_3$ shifted the maximum of DTG curve to lower value. This finding can be explained with the catalytic effect of Na^+ similarly to the observations described in the literature [68].

Results of Raman spectroscopic measurements (Figure 7) confirmed the almost exclusive formation of rutile TiO_2 polymorph even after drying at 85 °C.

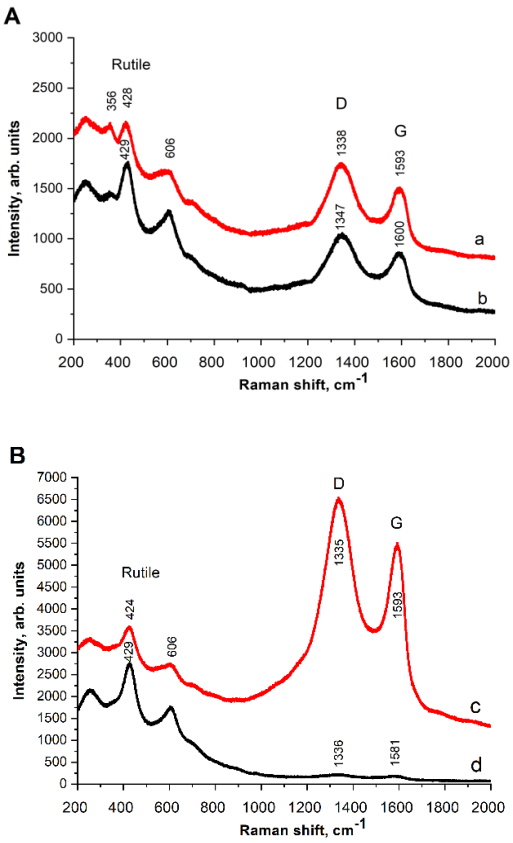

Fig. 7 Raman spectra of GO derived composites before (A) and after HTT (B). **a**: TiGO-2, **b**: TiGO-3, **c**: TiGO-2HT, **d**: TiGO-3HT.

The presence of GO derived carbon in the composites has been demonstrated by the corresponding D and G bands of graphene [69]. The D band corresponds to the breakdown of translational symmetry generated by the microcrystalline structure, while the G band is assigned to the Raman-active E_{2g} mode for the tangential in-plane stretching vibrations of the sp^2-hybridized bond [70]. The I_D/I_G ratio is a measure of the degree of defects present in the sample and the in-plane crystalline size of the sample. The I_D/I_G ratio was 1.89 in case of both TiGO-2 and TiGO-3 samples reflecting the same degree of the defect of graphene sheet by use of the same starting carbonaceous material (GO(II)). The intensity ratios of bands belonging to crystalline TiO_2 phase and bands belonging to the GO part was also very similar in these two composites which indicated that the Na removal did not result in significant differences in the samples dried at low temperature. However, I_D/I_G ratios of the samples after HTT were different, 1.27 and 2.06 for TiGO-2HT and TiGO-3HT, respectively. Furthermore, the intensity ratios of the bands characteristic for GO and the rutile TiO_2 in the washed and unwashed samples differed significantly after HTT. Beside the changes in intensity ratios, the G and D position were also shifted as a result of the HTT in case of the unwashed sample. These

observations indicated the different amount/quality of carbonaceous part and the different degree of crystallization.

Results of XPS study of sample TiGO-2HT and TiGO-3HT along with those of the BP carbon based TiBPHT are shown in Table 3.

Table 3. Comparison of unwashed and washed composite supports

Sample	$NaNO_3$ removal	XPS			EDX
		Composition in at %	Oxide/C content in wt.%[a]	Na/Ti	Na/Ti
TiGO-2HT	No	Ti: 7.3 O: 30.3 C: 52.9 Na: 9.5	63/37	1.30	0.075
TiGO-3HT	yes	Ti: 5.0 O: 16.3 C: 78.7 Na: --	36/64	0.00	0.000
TiBPHT	n.r.[b]	Ti: 7.0 O: 19.8 C: 73.2 Na: --	43/57	0.00	0.000

[a]nominal oxide/carbon content: 75/25 weight%;
[b]n.r.: not relevant.

Sodium appeared only in the TiGO-2HT sample which was obtained without nitric acid wash prior to HTT. The Na 1s peak appeared at 1072.1 eV binding energy. This value, along with the 990.4 eV kinetic energy of the Na KLL Auger line (resulting in an Auger parameter of 2062.5 eV) indicated that sodium was present in oxide form on the surface after the HTT. Presence of Na-nitrate compounds could be ruled out as no nitrogen signal was observed in the TiGO-2HT sample. The surface carbon content of the unwashed sample was lower than that of the washed one while the surface oxygen content of the unwashed sample was higher than that of the washed one. Na/Ti ratio obtained by EDX was in line with the XPS data (Table 3). These findings were consistent with the supposed burning effect of the $NaNO_3$ decomposition during the HTT. In conclusion, it can be stated that $NaNO_3$ can be successfully removed with the washing step we introduced, thus replacing the long pre-purifying of GO, too.

3.3 Characterization of selected TiO_2-C supports and 20 wt.% Pt/TiO_2-C electrocatalysts

3.3.1 Physicochemical characterization

N_2 physisorption behavior of selected supports representing both the GO derived (TiGO-3HT) and BP derived (TiBPHT) samples are shown in Figure 8 and Table S1 in the

Supplementary Materials. The shape of the isotherms recorded over the composite supports obtained from different types of parent carbonaceous materials differed significantly (*cf*. Figure 8A and 8B).

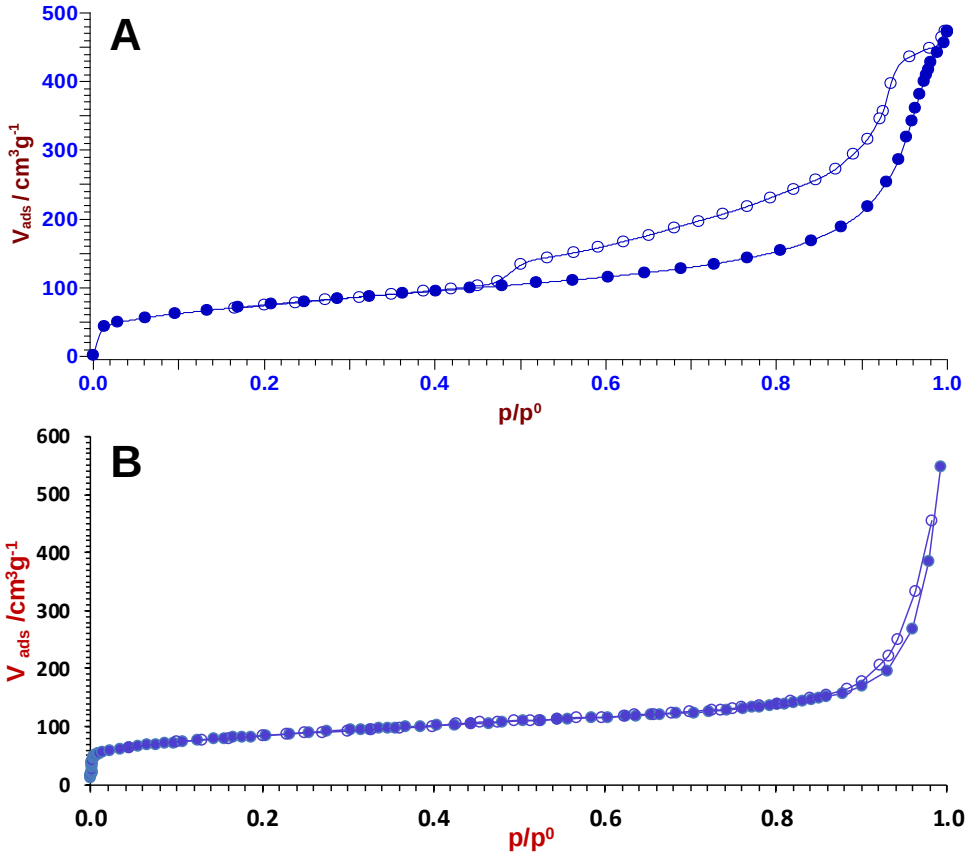

Fig. 8 Adsorption isotherm of selected TiO_2-C supports A: TiGO-3HT, B: TiBPHT

Isotherms of TiGO-3HT (Figure 8A) had typical H3 type of hysteresis loop according the UPAC classification [71], which suggests the presence of aggregated flat particles and reflects the structure of the parent carbonaceous material, *i.e.* the graphene-oxide sheets of the delaminated GO. TiGO-1STHT (not shown) had similar pattern. Mesopores were characteristic for samples TiGO-3HT and TiGO-1STHT, the volume of micropores were almost negligible (Table S1 in the Supplementary Materials). Because of the loop type of H3 pore size distribution could not be obtained for these samples. However, the BP derived sample (TiBPHT) showed very narrow H3 type of hysteresis loop (Figure 8B) indicating that mesopores were not characteristic for this composite but certain amount of micropores were present. Pore size distribution of sample TiBPHT was given in Figure S6. According to Figure S6 the maximum pore diameter of micropores was 0.16 nm. It could also be seen that the volume of micropores (which are unfavorable) was significantly reduced by the high (~75 wt.%) oxide content

compared to the parent BP carbon. The difference of the total pore volume and micropore volume (see in Table S1) could be attributed to the macropore volume or the volume between the particles in the TiBPHT sample.

BET specific surface area (S_{BET}) of the TiO_2-C composite types of samples was significantly lower than that of the parent BP carbon (Table 4). S_{BET} of TiBPHT and TiGO-3HT samples was similar to each other, but that of TiGO-1STHT was much lower. Therefore, platinum was loaded only onto the former two and electrochemical characterization was made only over this two composite supported catalyst.

Table 4. Some characteristic features of selected samples. Nominal value of TiO_2/C: 75/25

Sample ID	Support (HT)		Catalyst (Cat)
	Pore volume, cm^3g^{-1}	BET surface area, m^2g^{-1}	Pt based on ICP, wt.%
TiBPHT (Cat)	0.60 [a]	300	18.3
TiGO-3HT (Cat)	0.69	264	18.2
TiGO-1STHT	0.46	198	-
Parent BP [72]	0.59[b]	1635	-

[a]maximum pore diameter of micropores: 0.16 nm; [b]micropore volume

The introduction of Pt did not change the crystalline phase compared to the parent TiO_2-C composite (*cf.* line **f** in Figure 6 and line **a** in Figure 9); both TiGO-3Cat and TiBPCat electrocatalysts contained rutile phase and nanodispersed Pt indicated by a broad band at 40 degree in the XRD pattern (Figure 9).

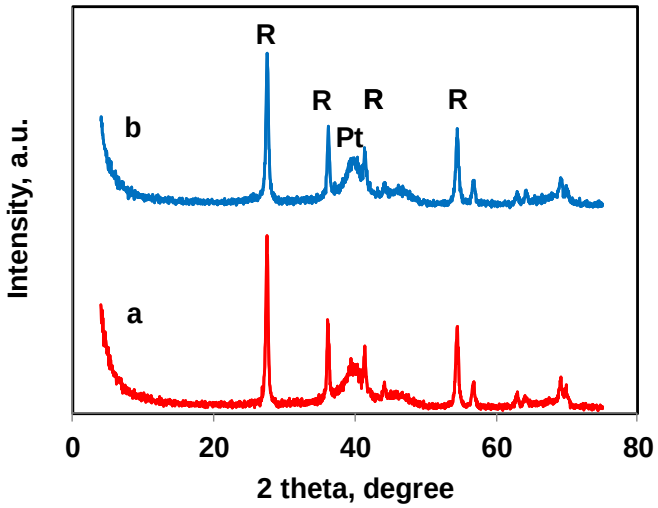

Fig. 9 XRD pattern of selected composite supported catalysts. A: TiBPCat, B: TiGO-3Cat, R: rutile.

Our previous works repeatedly demonstrated that this feature arises from well dispersed uniformly distributed Pt particles with average size around 2-3 nm [35,36,73]. Fine dispersion of Pt was mainly related to the applied modified sodium borohydride ($NaBH_4$) assisted ethylene-glycol (EG) reduction-precipitation method and to a lesser extent depended on the structural characteristics of the support [36]. The micrograph in Figure 10 also indicates the presence of finely dispersed Pt nanopatrticles both on the surface of TiBPCat (Figure 10A) and TiGO-3Cat (Figure 10B) samples. The ICP measured Pt content (Table 4) showed good agreement with the nominal value of 20 wt.%.

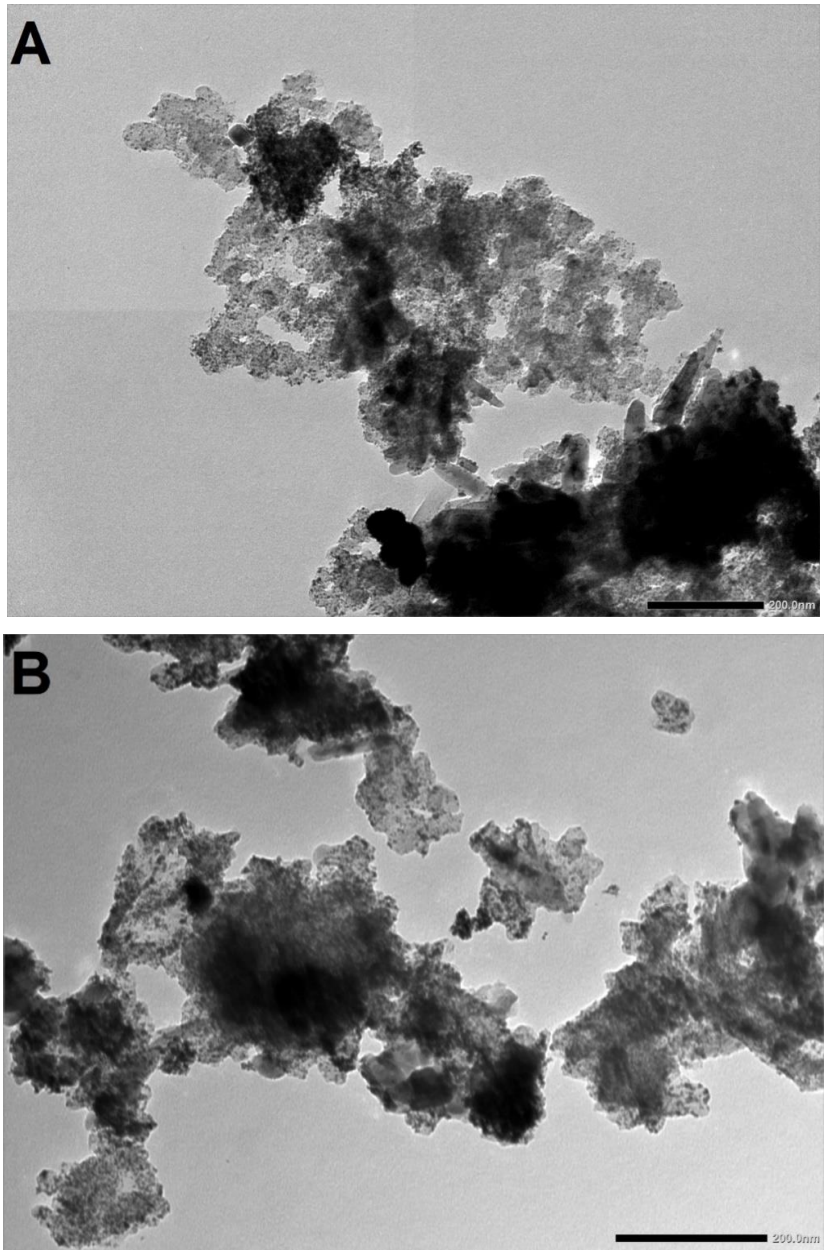

Fig. 10 TEM images of selected composite supported catalysts. A: TiBPCat, B: TiGO-3Cat (bar: 200 nm)

3.3.2 Electrochemical characterization

The effect of the type of carbonaceous materials on the electrochemical properties of the TiBPCat and TiGO-3Cat electrocatalysts was studied by cyclic voltammetry, CO_{ads}-stripping voltammetry and ORR measurements. The results obtained on fresh catalysts and after the 500 and 10,000 polarization cycles of the stability test were shown in Table 5. For comparison, the results of the study of commercial 20 wt.% Pt/C (Quintech) catalyst presented in Ref. [36] were also included.

Table 5. Electrochemical characterization of the 20 wt.% Pt/TiO_2-C electrocatalysts.

Sample	**$E_{CO,max}$, [a)] mV**	**$ECSA_1$, m^2/g_{Pt} [b)]**	**$\Delta ECSA_{500}$, % [c)]**	**$\Delta ECSA_{10,000}$, % [c)]**
TiGO-3Cat	775 (sh: 705)	82.9	6.4	34.3
TiBPCat	775 (sh: 705)	82.0	7.0	39.9
Pt/C [c)]	795	94.5	12.7	47.8

[a)] The position of the main CO stripping peak and shoulder in brackets (***sh***) obtained on fresh catalysts;

[b)] $ECSA_1$ means ECSA determined from the first polarization cycle

[b)] $\Delta ECSA_N = \{1-(ECSA_N/ECSA_1)\}\times 100\%$ (Equation S2, Supplementary Materials);

[c)] From Ref. [36].

Cyclic voltammograms obtained on fresh catalysts and after 500-cycle stability test are presented on Figures 11A and 11B, respectively. Figures 11A and 11B show that the shape of the voltammograms of both TiO_2-C composite supported Pt catalysts obtained before and after 500-cycle stability test was very similar: TiBPCat and TiGO-3Cat samples demonstrate a typical voltammogram characteristic for Pt in acid electrolytes. In good agreement with the literature data [74], on the voltammograms of the TiO_2-containing catalysts only the classical features of the underpotentially deposited hydrogen adsorption/desorption between 50 mV and 350 mV were observed, indicating that the TiO_2 was electrochemically inert.

It is necessary to mention that high oxide content in the electrocatalyst layer used in the preparation of membrane electrode assembly (MEA) can lead to an increase of the internal resistance of the cell and, as a consequence, in a decrease of the fuel cell performance [75]. Thus, Wang *et al*. [12] demonstrated that as a result of electronic resistance increase, the ECSA of the Pt/graphene-TiO_2 catalysts significantly decreased from 77.4 to 12.3 m^2/g with increasing TiO_2 content in the composite from 20 to 60 wt.%, respectively.

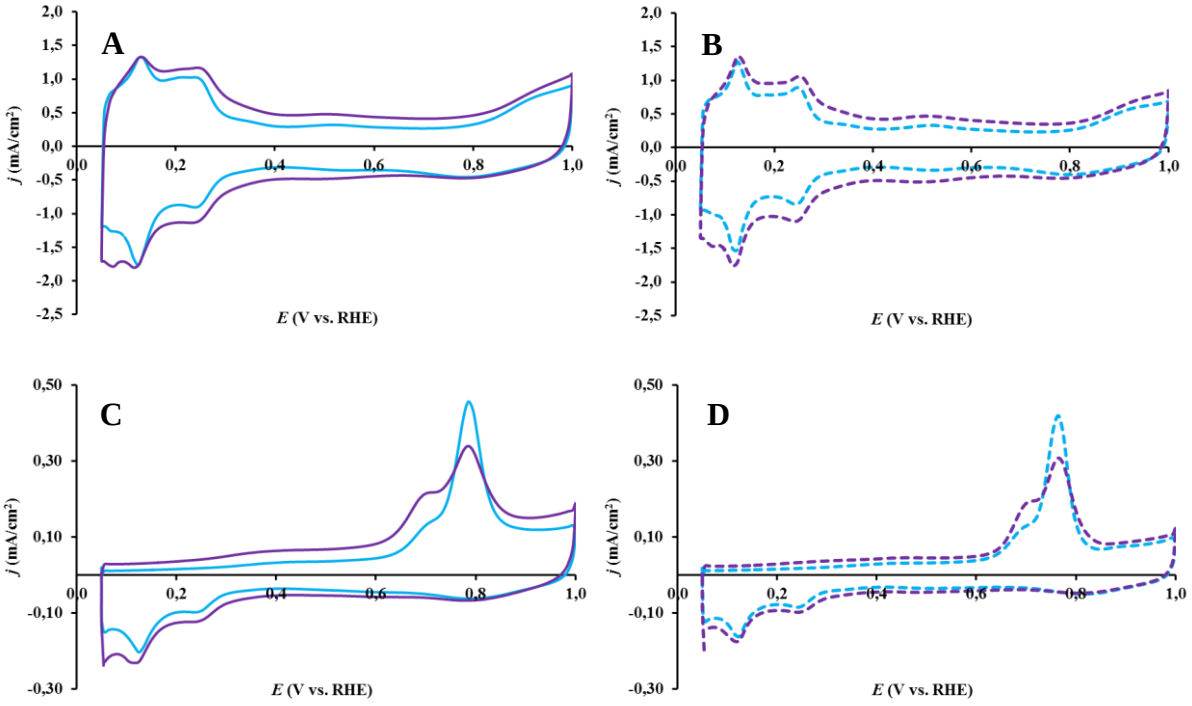

Fig. 11 Cyclic voltammograms and CO_{ads} stripping voltammograms of the electrocatalysts recorded in 0.5 M H_2SO_4 before (A, C: solid curves) and after 500 cycles (B, D: dashed curves) of the stability test: TiBPCat ( ) and TiGO-3Cat ( ). Sweep rate: 100 mV/s (A, B) and 10 mV/s (C, D).

As can be seen from Figures 11A and 11B, despite the presence of high content of TiO_2 oxide in the TiBPCat and TiGO-3Cat catalysts (75 weight%), well-defined characteristic peaks of hydrogen adsorption/desorption on Pt was observed in the potential range between 50 <E < 350 mV. This result is quite important as low electrochemically active Pt surface area is a common problem of oxide supported electrocatalysts. We have previously demonstrated [36] that when preparing catalysts with high surface area carbon, the carbonaceous backbone behaves like a good hard template, resulting in a uniform distribution of platinum over support even at high loading of active metal. These results suggest that catalysts with a very similar phase composition can be prepared using different carbonaceous materials and an optimized synthesis method. Moreover, these observations are in good agreement with XPS results, demonstrating that the carbonaceous material in the GO derived carbon based composite seems to be very similar to that in the BP carbon based material.

It should be noted that the literature is somewhat controversial on the question concerning to an optimal oxide/carbon ratio in the composites and stability of related electrocatalysts. Thus, upon investigation of the Pt/TiO_2-C catalysts with different TiO_2 loadings (10, 30 and 60 wt.%) the highest stability was obtained on the catalyst with 10 wt.%

TiO_2 content [9], but in Ref. [76], taking into account activity and stability of various catalysts, 40 weight% of oxide in the composite TiO_2-C support was chosen as optimal.

The electrochemically active surface area of Pt obtained on fresh catalysts was determined by charge integration under the hydrogen desorption peaks appearing between 50 mV and 350 mV according to Equation S1 (see Table 5). The $\Delta ECSA_{500}$ and $\Delta ECSA_{10,000}$ values calculated using the Equation S2 were also included.

The ECSAs of both TiO_2-containing composite supported catalysts, normalized by the initial value, were presented in Figure 12.

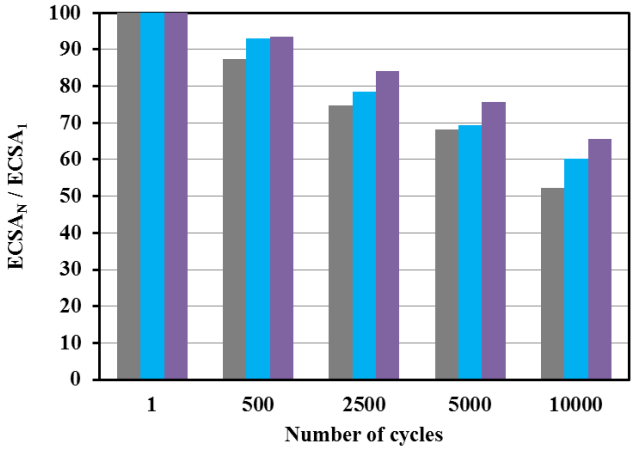

Fig. 12 Electrochemical long-term stability test: comparison of the electrochemically active Pt surface area measured after N cycles normalized to ECSA measured in the 1st cycle ($ECSA_N/ECSA_1$) of the TiBPCat ( ) and TiGO-3Cat ( ) catalysts as a function of the number of cycles (N); results obtained in Ref. [36] on the reference 20 wt.% Pt/C catalyst ( ) are given for comparison.

As can be seen from Figure 12, all catalysts exhibited some decrease of ECSA with increased cycle number. After 10,000 polarization cycles in the potential range 50 <E < 1000 mV, the TiGO-3Cat catalyst seems to be the most promising; the loss in the electrochemical surface area (ΔECSA) increased in the following order: TiGO-3Cat < TiBPCat < Pt/C.

As shown in Table 5 the reference Pt/C catalyst showed the highest degradation after the 10,000-cycle stability test (~ 48%). However, it should be emphasized that during the CV measurements these catalysts were exposed to quite mild corrosive conditions, so the difference in the ΔECSA values of Pt/C and TiO_2-containing composite supported catalysts was not so noticeable.

These results are in good agreement with the literature data, since it is generally accepted that under these conditions (at potentials ≤ 1.0 V), a Pt reference catalyst supported on high-surface-area carbon support usually corrodes to a rather insignificant extent [74,77,78].

It should be noted, that pronounced difference in the stability of reference Pt/C and TiO_2-C composite supported Pt catalysts can be observed only under conditions, which simulates start/stop conditions in fuel cells: potential cycles between 1.0 and 1.5 V vs. RHE.

Results presented on Figure 12 obtained on the Pt/C and Pt/TiO_2-C catalysts are consistent with the results obtained by Zana *et al*. [4] when comparing the stability of the Pt/TiO_2@C, Pt/TiO_2 and Pt/C catalysts under start/stop cycles and much milder load cycles conditions (cycling the potential between 0.6 and 1.0 V RHE). It has been proposed [4] that the catalyst stability under mild load cycles mainly depends on the properties of the active phase (e.g. Pt NPs), while under start/stop cycles the support properties determine the stability.

As shown in Figure 11C the character of CO_{ads} stripping voltammograms of both electrocatalysts supported either on BP derived composite (TiBPCat) or GO derived one (TiGO-3Cat) were quite similar; no significant difference in the shape of the main CO oxidation peak and the location of the maximum of this peak was observed on these catalysts.

It is well established that creating ensemble sites consisting of Pt and a second oxophilic metal, which facilitates easy oxidation of the CO contaminant via the bifunctional mechanism, is a viable method for decreasing the sensitivity of the Pt/C electrocatalysts towards CO poisoning [7,74, 79-81]. In this respect the position of the CO_{ads} electrooxidation peaks can reflect the degree of the interaction between the Pt nanoparticles and oxophilic metal-containing support.

As can be seen from the results presented in Table 5 the maximum of the main CO oxidation peak on the CO_{ads}-stripping voltammogram of both fresh samples appeared at 775 mV, at a slightly less positive potential value than on that of the Pt/C (~795 mV). It is necessary to mention that besides the main CO_{ads}-stripping peak, a small pre-oxidation peak (shoulder) at 705 mV was also observed on both TiO_2-containing catalysts, but in the case of the TiGO-3Cat sample, this pre-oxidation peak was more pronounced.

This behavior and shape of the CO_{ads}-stripping curves, demonstrating increased tolerance towards CO poisoning, are characteristic of Pt/TiO_2-C electrocatalysts and have already been described in the literature as a unique Pt-TiO_2-carbon three phase junction structure, which forms two types of Pt active sites: the former are associated with active OH_{ads} on the TiO_2 surface, giving a pre-oxidation peak, while the latter are associated with the surface of carbonaceous materials responsible for the appearance of the main peak [28, 82-83]. Thus,

in Ref. [6] the increased CO tolerance of the Pt/graphene-TiO_2 catalyst as compared to Pt/graphene was associated with the synergetic effect of these three components. It has been demonstrated by Kuriganova *et al*. [9] that the presence of 10 % TiO_2 or more (30, 60 %) in the Pt/TiO_2-C electrocatalyst obtained *via* electrochemical oxidation/dispersion causes a decrease of the onset potential and in a shift of the position of the main CO oxidation peak by 70–100 mV toward less positive potential values as compared to that obtained on Pt/C catalyst.

Obviously, the presence of stable TiO_2 coatings on a carbon support is one of the most important factors ensuring the high resistance of catalysts to CO poisoning. In this respect, significant sintering of titania during high-temperature treatment, observed by XPS and TEM, which leads to the formation of relatively large TiO_2 crystallites and incomplete coverage of the carbon backbone, may be the reason that, despite the high content of TiO_2 oxide in the TiO_2-C composite, the contribution of CO oxidation occurring at the Pt-C interface is significant especially in the case of TiBPCat.

It should be noted that the presence of two electrooxidation peaks could also be attributed to inhomogeneous Pt particle size distribution according to literature analogies [84,85]. Thus, in Refs. [84,85] the presence of two overlapping peaks of CO_{ads} electrooxidation was attributed to CO oxidation on agglomerated Pt nanoparticles of various structures with high density of surface defects.

The effect of the 500-cycle stability test performed in the potential range between 50 and 1000 mV on the shape of the CO_{ads}-stripping voltammograms was presented in Figure 11D. After stability test the main CO stripping peak on both TiO_2-containing composite supported catalysts was shifted ~10 mV in the direction of less positive potential values compared to that obtained on fresh samples, which may be due to some agglomeration of Pt nanoparticles [84].

The results obtained on the TiO_2-C composite supported 20 wt.% Pt catalysts were compared with the results of the study of the Mo-containing 20 wt.% Pt/ $Ti_{0.8}Mo_{0.2}O_2$-C (C= BP and GO derived) catalysts presented in Ref. [36] (see Table S2 in Supplementary Materials).

As can be seen from Table S2, the addition of Mo to composites obtained using carbonaceous materials of a certain type and the same oxide/carbon ratio does not affect the ECSA and the stability of the related Pt electrocatalysts. Nevertheless, it is obvious that the presence of molybdenum in the catalyst increases the CO tolerance to a significant extent, which is reflected by a shift in the position of the main CO_{ads} stripping peak on the Mo-containing Pt/75 wt.% $Ti_{0.8}Mo_{0.2}O_2$-25 wt.% C catalysts to 705 mV and the appearance of the so-called “pre-peak” (see Supplementary Materials for more details).

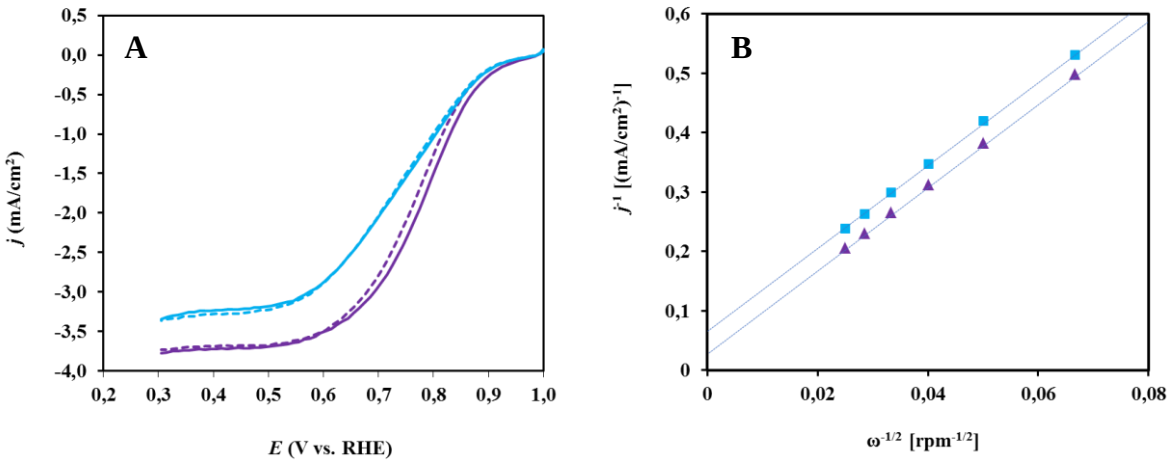

Figure 13. (A) Oxygen reduction reaction polarization curves of the TiBPCat (■) and TiGO-3Cat (■) catalysts obtained in O_2-saturated 0.5 M H_2SO_4 on a RDE at 900 rpm before (solid line) and after (dashed line) 500 cycles of the stability test. *j* vs. *E* curves were obtained during cathodic scan at 10 mV s^{-1} sweep rate. (B) Koutecky - Levich representation of ORR measurements obtained on these catalysts.

Catalytic activity in the ORR after 10 cycles of conditioning of the TiBPCat and TiGO-3Cat electrocatalysts obtained before and after 500-cycle stability test was investigated by RDE technique. As shown in Fig. 13.A, current density of the ORR in the mixed kinetic-diffusion controlled region on the fresh GO-derived TiGO-3Cat catalyst was higher comparing to the TiBPCat catalyst, whereas the limiting current of the TiBPCat catalyst was slightly lower (the difference in saturation currents may reflect a difference in the mass transport properties of the catalyst layers). As can be seen from Figure 13.A, both catalysts retain good stability after 500 polarization cycles in the potential range of 50 <E < 1000 mV.

The dependency of the current densities on the rotating rates at low potentials indicates that the diffusion limited nature of the oxygen reduction. Fig. 13.B depicts the relationship between the the square root of the rotation speed and the current density at 300 mV potential for both catalysts (Koutecky - Levich plot). Apart from confirming the reliability of the RDE measurements, as indicated by the linearity of the plots, the similar slopes of the curves suggest that the ORR proceeds with the same reaction mechanism on these catalysts.

4. Summary

Our previously developed sol-gel method for the preparation of the mixed oxide- carbon composite type of electrocatalyst support was successfully adapted to the use of GO derived carbonaceous material. In order to get GO derived TiO_2-C composite material containing rutile TiO_2, the following difficulties had to be overcome: (1) strong acidic media adjusted by HNO_3

was necessary for the formation of the rutile nuclei; while media of much higher pHs (added NaOH) was useful for the delamination of GO. It was proved by XRD measurements that addition of 5 hours aged solution of Ti(O-*i*-Pr)$_4$ to delaminated GO under vigorous stirring resulted in exclusively the rutile phase of the oxide after HTT. (2) Crystalline $NaNO_3$ was formed by use of the delaminated GO in the conventional composite preparation method of the research team. During HTT, which is necessary for the crystallization of the rutile TiO_2 phase, this $NaNO_3$ decomposed leading to uncontrolled treatment conditions. XRD and XPS measurements proved that by use of an acidic wash $NaNO_3$ could be removed. As $NaNO_3$ can also be a contaminant of the parent GO material, this result indicates that the acidic wash can replace the more expensive dialysis for GO purification. ^{13}C NMR and TEM measurements proved that the carbon structure of the solvothermally treated sample differed significantly from that obtained without solvothermal treatment.

Based on the results of XPS and TEM, it can be concluded that, regardless of the carbon source, sintering of titania during high-temperature treatment of TiO_2-C composites leads to the formation of relatively large crystallites with incomplete coverage of the carbon backbone. In good agreement with these results, electrochemical studies have shown that the presence of the 75 weight% TiO_2 in the BP and GO-derived TiO_2-C composite does not significantly affect the performance of related Pt catalysts. Long-term stability tests carried out in the potential range 50 <E < 1000 mV showed that the stability of catalysts under these conditions mainly depends on the properties of the active phase (i.e., Pt NPs), while the effect of the composite support is limited. The Pt/TiO_2-GO derived sample showed higher ORR activity than the Pt/TiO_2-BP derived one. Based on the decrease of electrochemical surface area, the stability order was the following: Pt/C (commercial) < Pt/TiO_2-BP derived C < Pt/TiO_2-GO derived C.

References

[1] Bharath G, Prakash J, Rambabu K, et al (2021) Synthesis of TiO_2/RGO with plasmonic Ag nanoparticles for highly efficient photoelectrocatalytic reduction of CO_2 to methanol toward the removal of an organic pollutant from the atmosphere. Environ Pollut 281:116990. https://doi.org/10.1016/j.envpol.2021.116990

[2] Elbakkay MH, El Rouby WMA, El-Dek SI, et al (2018) S-TiO_2/S-reduced graphene oxide for enhanced photoelectrochemical water splitting. Appl Surf Sci 439:1088−1102. https://doi.org/10.1016/j.apsusc.2018.01.070

[3] Yu J, Liu Z, Zhai L, et al (2016) Reduced graphene oxide supported TiO_2 as high performance catalysts for oxygen reduction reaction. Int J Hydrogen Energy 41:3436−3445. http://dx.doi.org/10.1016/j.ijhydene.2015.12.192

[4] Zana A, Rüdiger C, Kunze-Liebhäuser J, et al (2014) Core-shell TiO_2@C: Towards alternative supports as replacement for high surface area carbon for PEMFC catalysts. Electrochim Acta 139:21–28. http://dx.doi.org/10.1016/j.electacta.2014.07.002

[5] Li Y, Liu C, Liu Y, et al (2015) Sn-doped TiO_2 modified carbon to support Pt anode catalysts for direct methanol fuel cells. J Power Sources 286:354–361. http://dx.doi.org/10.1016/j.jpowsour.2015.03.155

[6] Zhao L, Wang ZB, Liu J, et al (2015) Facile one-pot synthesis of Pt/graphene-TiO_2 hybrid catalyst with enhanced methanol electrooxidation performance. J Power Sources 279:210–217. http://dx.doi.org/10.1016/j.jpowsour.2015.01.023

[7] Zhuang W, He L, Zhu J, et al (2015) TiO_2 nanofibers heterogeneously wrapped with reduced graphene oxide as efficient Pt electrocatalyst supports for methanol oxidation. Int J Hydrogen Energy 40:3679−3688. http://dx.doi.org/10.1016/j.ijhydene.2015.01.042

[8] Wu X, Zhuang W, Lu L, et al (2017) Excellent performance of Pt-C/TiO_2 for methanol oxidation: Contribution of mesopores and partially coated carbon. Appl Surf Sci 426:890–896. http://dx.doi.org/10.1016/j.apsusc.2017.07.219

[9] Kuriganova AB, Leontyev IN, Alexandrin AS, et al (2017) Electrochemically synthesized Pt/TiO_2-C catalysts for direct methanol fuel cell applications. Mendeleev Commun 27:67–69. https://doi.org/10.1016/j.mencom.2017.01.021

[10] Odetola C, Trevani LN, Easton EB (2017) Photo enhanced methanol electrooxidation: Further insights into Pt and TiO_2 nanoparticle contributions. Appl Catal B Environ 210:263–275. https://doi.org/10.1016/j.apcatb.2017.03.027

[11] Fan Y, Yang Z, Huang P, et al (2013) Pt/TiO_2−C with hetero interfaces as enhanced catalyst for methanol electrooxidation, Electrochim Acta 105:157– 161. http://dx.doi.org/10.1016/j.electacta.2013.04.158

[12] Wang M, Wang Z, Wei L, et al (2017) Catalytic performance and synthesis of a Pt/graphene-TiO_2 catalyst using an environmentally friendly microwave-assisted solvothermal method. Chinese J Catal 38:1680–1687. DOI: 10.1016/S1872-2067(17)62876-6

[13] Zhang H, Han X, Zhao Y (2017) Pd-TiO_2 nanoparticles supported on reduced graphene oxide: Green synthesis and improved electrocatalytic performance for methanol oxidation. J Electroanal Chem 799:84–91. http://dx.doi.org/10.1016/j.jelechem.2017.05.02

[14] Li M, Bi YG, Xiang L, et al (2020) Improved cathodic oxygen reduction and bioelectricity generation of electrochemical reactor based on reduced graphene oxide decorated with titanium-based composites. Bioresour Technol 296:122319. https://doi.org/10.1016/j.biortech.2019.122319

[15] Shim J, Lee CR, Lee HK, et al (2001) Electrochemical Characteristics of Pt-WO_3/C and Pt-TiO_2/C electrocatalysts in a polymer electrolite fuel cell. J Power Source 102:172-171. DOI:10.1016/S0378-7753(01)00817-5

[16] Zeng X, Wang Z, Meng N, et al (2017) Highly dispersed TiO_2 nanocrystals and carbon dots on reduced graphene oxide: Ternary nanocomposites for accelerated photocatalytic water disinfection. Appl Catal B Environ 202:33–41. http://dx.doi.org/10.1016/j.apcatb.2016.09.014

[17] Sravani B, Chandrashekar Y, Chandana PS, et al (2020) Bimetallic PtCu-decorated reduced graphene oxide (RGO)-TiO_2 nanocomposite for efficient oxygen reduction reaction. Synt Met 266:116433. https://doi.org/10.1016/j.synthmet.2020.116433

[18] Li F, Long L, Weng Y (2020) A Review on the Contemporary Development of Composite Materials Comprising Graphene/Graphene Derivatives. Adv Mater Sci Eng 2020:7915641. https://doi.org/10.1155/2020/7915641

[19] Szabó T, Tombácz E, Illés E, et al (2006) Enhanced acidity and pH-dependent surface charge characterization of successively oxidized graphite oxides. Carbon N Y 44:537–545. https://doi.org/10.1016/j.carbon.2005.08.005

[20] Szabó T, Berkesi O, Forgó P, et al (2006) Evolution of surface functional groups in a series of progressively oxidized graphite oxides. Chem Mater 18:2740–2749. https://doi.org/10.1021/cm060258+

[21] Lerf A, He H, Forster M, et al (1998) Structure of graphite oxide revisited. J Phys Chem B 102:4477–4482. https://doi.org/10.1021/jp9731821

[22] Zhang N, Yang MQ, Liu S, et al (2015) Waltzing with the Versatile Platform of Graphene to Synthesize Composite Photocatalysts. Chem Rev 115:10307–10377. https://doi.org/10.1021/acs.chemrev.5b00267

[23] Park Y, Kang SH, Choi W (2011) Exfoliated and reorganized graphite oxide on titania nanoparticles as an auxiliary co-catalyst for photocatalytic solar conversion. Phys Chem Chem Phys 13:9425–9431. https://doi.org/10.1039/c1cp20697d

[24] Nagaraju G, Manjunath K, Sarkar S, et al (2015) TiO_2-RGO hybrid nanomaterials for enhanced water splitting reaction Dedicated to 108th Birthday (born April 1, 1907) of Dr. Sree Sree Sree Shivakumara Mahaswamiji, Siddaganga Matta, Tumakuru, Karnataka, India. Int J Hydrogen Energy 40:12209–12216. https://doi.org/10.1016/j.ijhydene.2015.07.094

[25] Szabó T, Veres Á, Cho E, et al (2013) Photocatalyst separation from aqueous dispersion using graphene oxide/TiO_2 nanocomposites. Colloids Surfaces A Physicochem Eng Asp 433:230–239. https://doi.org/10.1016/j.colsurfa.2013.04.063
[26] Majrik K, Turcsányi Á, Pászti Z, et al (2018) Graphite Oxide-TiO_2 Nanocomposite Type Photocatalyst for Methanol Photocatalytic Reforming Reaction. Top Catal 61:1323–1334. https://doi.org/10.1007/s11244-018-0989-z
[27] Zhang X, Liu Q, Shi X, et al (2018) TiO_2 nanoparticles-reduced graphene oxide hybrid: An efficient and durable electrocatalyst toward artificial N_2 fixation to NH_3 under ambient conditions. J Mater Chem A 6:17303–17306. https://doi.org/10.1039/c8ta05627g
[28] Qu Y, Gao Y, Kong F, et al (2013) Pt−rGO−TiO_2 nanocomposite by UV photoreduction method as promising electrocatalyst for methanol oxidation. Int J Hydrogen Energy 38:12310−12317. http://dx.doi.org/10.1016/j.ijhydene.2013.07.038
[29] Yuan W, Li J, Wang L, et al (2014) Nanocomposite of N-doped TiO_2 nanorods and graphene as an effective electrocatalyst for the oxygen reduction reaction. ACS Appl Mater Interfaces 6:21978–21985. https://doi.org/10.1021/am507890h
[30] Cai Z, Bu X, Wang P, et al (2019) Recent advances in layered double hydroxide electrocatalysts for the oxygen evolution reaction. J Mater Chem A 7:5069–5089. DOI: 10.1039/c8ta11273h
[31] Xie X, Chen S, Ding W, et al (2013), An extraordinarily stable catalyst: Pt NPs supported on two-dimensional $Ti_3C_2X_2$ (X = OH, F) nanosheets for oxygen reduction reaction. Chem Commun 49:10112–10114. DOI: 10.1039/c3cc44428g
[32] Peera SG, Liu C, Shim J, et al (2021) MXene ($Ti_3C_2T_x$) supported electrocatalysts for methanol and ethanol electrooxidation: A review. Ceram Int, in press https://doi.org/10.1016/j.ceramint.2021.07.075
[33] Vass Á, Borbáth I, Pászti Z, et al (2017) Effect of Mo incorporation on the electrocatalytic performance of Ti–Mo mixed oxide–carbon composite supported Pt electrocatalysts. React Kinet Mech Catal 121:141–160. https://doi.org/10.1007/s11144-017-1155-5
[34] Vass Á, Borbáth I, Bakos I, et al (2019) Stability issues of CO tolerant Pt-based electrocatalysts for polymer electrolyte membrane fuel cells: comparison of Pt/$Ti_{0.8}Mo_{0.2}O_2$–C with PtRu/C. React Kinet Mech Catal 126:679–699. https://doi.org/10.1007/s11144-018-1512-z

[35] Borbáth I, Zelenka K, Vass Á, et al (2021) CO tolerant Pt electrocatalysts for PEM fuel cells with enhanced stability against electrocorrosion. Int J Hydrogen Energy 46:13534–13547. https://doi.org/10.1016/j.ijhydene.2020.08.002

[36] Borbáth I, Tálas E, Pászti Z, et al (2021) Investigation of Ti-Mo mixed oxide-carbon composite supported Pt electrocatalysts: Effect of the type of carbonaceous materials. Appl Catal A Gen 620:118155. https://doi.org/10.1016/j.apcata.2021.118155

[37] Gubán D, Borbáth I, Pászti Z, et al (2015) Preparation and characterization of novel $Ti_{0.7}W_{0.3}O_2$-C composite materials for Pt-based anode electrocatalysts with enhanced CO tolerance. Appl Catal B-Environ 174:455-470. https://doi.org/10.1016/j.apcatb.2015.03.031

[38] Odetola C, Easton EB, Trevani L (2016) Investigation of TiO_2/carbon electrocatalyst supports prepared using glucose as a modifier. Int J Hydrogen Energy 41:8199–8208. https://doi.org/10.1016/j.ijhydene.2015.10.035

[39] Hakamizadeh M, Afshar S, Tadjarodi A, et al (2014) Improving hydrogen production via water splitting over Pt/TiO_2/activated carbon nanocomposite. Int J Hydrogen Energy 39:7262–7269. https://doi.org/10.1016/j.ijhydene.2014.03.048

[40] Odetola C, Trevani L, Easton EB (2015) Enhanced activity and stability of Pt/TiO_2/carbon fuel cell electrocatalyst prepared using a glucose modifier. J Power Sources 294:254–263. https://doi.org/10.1016/j.jpowsour.2015.06.066

[41] Guha A, Lu W, Zawodzinski TA, Schiraldi DA (2007) Surface-modified carbons as platinum catalyst support for PEM fuel cells. Carbon N Y 45:1506–1517. https://doi.org/10.1016/j.carbon.2007.03.023

[42] Zhang Q, He YQ, Chen XG, et al (2011) Structure and photocatalytic properties of TiO_2-Graphene Oxide intercalated composite. Chinese Sci Bull 56:331–339. https://doi.org/10.1007/s11434-010-3111-x

[43] Liang Y, Wang H, Casalongue HS, et al (2010) TiO_2 Nanocrystals grown on graphene as advanced photocatalytic hybrid materials. Nano Res 3:701–705. https://doi.org/10.1007/s12274-010-0033-5

[44] Xu C, Wang X, Zhu J (2008) Graphene - Metal particle nanocomposites. J Phys Chem C 112:19841–19845. https://doi.org/10.1021/jp807989b

[45] Kou R, Shao Y, Wang D, et al (2009) Enhanced activity and stability of Pt catalysts on functionalized graphene sheets for electrocatalytic oxygen reduction. Electrochem Commun 11:954–957. https://doi.org/10.1016/j.elecom.2009.02.033

[46] Rao CV, Reddy ALM, Ishikawa Y, et al (2011) Synthesis and electrocatalytic oxygen reduction activity of graphene-supported Pt_3Co and Pt_3Cr alloy nanoparticles. Carbon N Y 49:931–936. https://doi.org/10.1016/j.carbon.2010.10.056
[47] Hanaor DAH, Sorrell CC (2011) Review of the anatase to rutile phase transformation. J Mater Sci 46:855–874. https://doi.org/10.1007/s10853-010-5113-0
[48] Bourikas K, Kordulis C, Lycourghiotis A (2014) Titanium dioxide (anatase and rutile): surface chemistry, liquid-solid interface chemistry, and scientific synthesis of supported catalysts. Chem Rev 114:9754-823. dx.doi.org/10.1021/cr300230q
[49] Wu J, Xu M, Lei S, et al (2020) High electrocatalytic activity and stability of PtAg supported on rutile TiO_2 for methanol oxidation. Int J Hydrogen Energy 45:12815-12821. https://doi.org/10.1016/j.ijhydene.2020.03.015
[50] Gudkov MV, Bazhenov SL, Bekhli LS, et al (2018) Explosive Reduction of Graphite Oxide. Russ J Phys Chem B 12:860–868. https://doi.org/10.1134/S199079311805007X
[51] Boehm H-P, Scholz W (1965) Der „Verpuffungspunkt" des Graphitoxids. ZAAC - J Inorg Gen Chem 335:74–79. https://doi.org/10.1002/zaac.19653350107
[52] Szabó T, Szeri A, Dékány I (2005) Composite graphitic nanolayers prepared by self-assembly between finely dispersed graphite oxide and a cationic polymer. Carbon N Y 43:87–94. https://doi.org/10.1016/j.carbon.2004.08.025
[53] Zhang H, Lv X, Li Y, et al (2010) P25-graphene composite as a high performance photocatalyst. ACS Nano 4:380–386. https://doi.org/10.1021/nn901221k
[54] Zhang Y, Tang Z-R, Fu X, Xu Y-J (2010) TiO_2 Graphene Nanocomposites for Gas-Phase Photocatalytic Degradation of Volatile Aromatic Pollutant: Is TiO_2 Graphene Truly Different from Other TiO_2 Carbon Composite Materials? ACS Nano 4:7303–7314. https://doi.org /10.1021/nn1024219
[55] Pan X, Zhao Y, Liu S, et al (2012) Nanoparticle Composite Photocatalysts. ACS Appl Mater Interfaces 4:3944–3950. dx.doi.org/10.1021/am300772t
[56] Leong KH, Sim LC, Bahnemann D, et al (2015) Reduced graphene oxide and Ag wrapped TiO_2 photocatalyst for enhanced visible light photocatalysis. APL Mater 3:104503. https://doi.org/10.1063/1.4926454
[57] Zeng P, Zhang Q, Zhang X, Peng T (2012) Graphite oxide-TiO_2 nanocomposite and its efficient visible-light-driven photocatalytic hydrogen production. J Alloys Compd 516:85–90. https://doi.org/10.1016/j.jallcom.2011.11.140

[58] Vasilaki E, Georgaki I, Vernardou D, et al (2015) Ag-loaded TiO_2 /reduced graphene oxide nanocomposites for enhanced visible-light photocatalytic activity. Appl Surf Sci 353:865–872. https://doi.org/10.1016/j.apsusc.2015.07.056
[59] Vass Á, Borbáth I, Bakos I, et al (2018) Novel Pt Electrocatalysts: Multifunctional Composite Supports for Enhanced Corrosion Resistance and Improved CO Tolerance. Top Catal 61:1300–1312. https://doi.org/10.1007/s11244-018-0988-0
[60] Bard AJ (1976) Electroanalytical chemistry: a series of advances. Volume 9. M. Dekker, New York; Basel
[61] Borbáth I, Bakos I, Pászti Z, et al (2021) Design of SnPt/C cathode electrocatalysts with optimized Sn/Pt surface composition for potential use in Polymer Electrolyte Membrane Fuel Cells. Catal Today 366:20–30. DOI: 10.1016/j.cattod.2020.06.029.
[62] Roy N, Leung KT, Pradhan D (2015) Nitrogen Doped Reduced Graphene Oxide Based Pt-TiO_2 Nanocomposites for Enhanced Hydrogen Evolution. J Phys Chem C 119:19117–19125. https://doi.org/10.1021/acs.jpcc.5b03870
[63] Wang R, Tang Y, Xu M, et al (2018) Transfer Hydrogenation of Aldehydes and Ketones with Isopropanol under Neutral Conditions Catalyzed by a Metal-Ligand Bifunctional Catalyst [Cp∗Ir(2,2′-bpyO)(H_2O)]. J Org Chem 83:2274–2281. https://doi.org/10.1021/acs.joc.7b03174
[64] Talyzin AV, Solozhenko VL, Kurakevych OO, et al (2008) Colossal pressure-induced lattice expansion of graphite oxide in the presence of water. Angew Chemie - Int Ed 47:8268–8271. https://doi.org/10.1002/anie.200802860
[65] Yamada Y, Yasuda H, Murota K, et al (2013) Analysis of heat-treated graphite oxide by X-ray photoelectron spectroscopy. J Mater Sci 48:8171–8198. https://doi.org/10.1007/s10853-013-7630-0
[66] Bauer T, Laing D, Kröner U, et al (2009) Sodium nitrate for high temperature latent heat storage. 11th Int Conf Therm Energy Storage 1–8
[67] Navio JA, Macias M, Justo A, et al (1992) Thermal decomposition of sodium nitrite and sodium nitrate pre-adsorbed on TiO_2 surfaces. J Therm Anal 38:673-682. https://doi.org/10.1007/BF01979396
[68] Sebestyén Z, May Z, Réczey K, et al (2011) The effect of alkaline pretreatment on the thermal decomposition of hemp. J Therm Anal Calorim 105:1061–1069. https://doi.org/10.1007/s10973-010-1056-6
[69] Kudin KN, Ozbas B, Schniepp HC, et al (2008) Raman spectra of graphite oxide and functionalized graphene sheets. Nano Lett 8:36–41. https://doi.org/10.1021/nl071822y

[70] Tian Z, Liu C, Li Q, et al (2015) Nitrogen- and oxygen-functionalized carbon nanotubes supported Pt-based catalyst for the selective hydrogenation of cinnamaldehyde. Appl Catal A Gen 506:134–142. https://doi.org/10.1016/j.apcata.2015.08.023

[71] Sing KSW, Williams RT (2004) Physisorption hysteresis loops and the characterization of nanoporous materials. Adsorpt Sci Technol 22:773–782. https://doi.org/10.1260/0263617053499032

[72] Pantea D, Darmstadt H, Kaliaguine S, et al (2003) Electrical conductivity of conductive carbon blacks: Influence of surface chemistry and topology. Appl Surf Sci 217:181–193. https://doi.org/10.1016/S0169-4332(03)00550-6

[73] Yazici MS, Dursun S, Borbáth I, Tompos A (2021) Reformate gas composition and pressure effect on CO tolerant Pt/$Ti_{0.8}Mo_{0.2}O_2$–C electrocatalyst for PEM fuel cells. Int J Hydrogen Energy 46:13524–13533. https://doi.org/10.1016/j.ijhydene.2020.08.226

[74] Huang SY, Ganesan P, Popov BN (2011) Titania supported platinum catalyst with high electrocatalytic activity and stability for polymer electrolyte membrane fuel cell. Appl Catal B: Environ 102:71–77. doi:10.1016/j.apcatb.2010.11.026

[75] von Kraemer S, Wikander K, Lindbergh G, et al (2008) Evaluation of TiO_2 as catalyst support in Pt-TiO_2/C composite cathodes for the proton exchange membrane fuel cell. J Power Sources 180:185–190. https://doi.org/10.1016/j.jpowsour.2008.02.023

[76] Jiang ZZ, Gu DM, Wang ZB, et al (2011) Effects of anatase TiO_2 with different particle sizes and contents on the stability of supported Pt catalysts. J Power Sources 196:8207–8215. https://doi.org/10.1016/j.jpowsour.2011.05.063

[77] Huang SY, Ganesan P, Park S, Popov BN (2009) Development of a titanium dioxide-supported platinum catalyst with ultrahigh stability for polymer electrolyte membrane fuel cell applications. J Am Chem Soc 131:13898–13899. https://doi.org/10.1021/ja904810h

[78] Ioroi T, Siroma Z, Fujiwara N, et al (2005) Sub-stoichiometric titanium oxide-supported platinum electrocatalyst for polymer electrolyte fuel cells. Electrochem commun 7:183–188. https://doi.org/10.1016/j.elecom.2004.12.007

[79] Yoo SJ, Jeon TY, Lee KS, et al (2010) Effects of particle size on surface electronic and electrocatalytic properties of Pt/TiO_2 nanocatalysts. Chem Commun 46:794–796. https://doi.org/10.1039/b916335b

[80] Ercelik M, Ozden A, Seker E, Colpan CO (2017) Characterization and performance evaluation of Pt-Ru/C-TiO_2 anode electrocatalyst for DMFC applications. Int J Hydrogen Energy 42:21518–21529. https://doi.org/10.1016/j.ijhydene.2016.12.020

[81] Chen C-S, Pan F-M (2009) Electrocatalytic activity of Pt nanoparticles deposited on porous TiO_2 supports toward methanol oxidation. Appl Catal B 91:663–669. doi:10.1016/j.apcatb.2009.07.008

[82] Zhao X, Zhu J, Liang L, et al (2012) Enhanced activity of Pt nano-crystals supported on a novel TiO_2@Ndoped C nano-composite for methanol oxidation reaction. J Mater Chem 22:19718-19725. DOI: 10.1039/c2jm33926a

[83] Song HQ, Qiu XP, Li FS (2008) Effect of heat treatment on the performance of TiO_2-Pt/CNT catalysts for methanol electro-oxidation. Electrochim Acta 53:3708-3713. doi:10.1016/j.electacta.2007.11.080

[84] Maillard F, Schreier S, Hanzlik M, et al (2005) Influence of particle agglomeration on the catalytic activity of carbon-supported Pt nanoparticles in CO monolayer oxidation. Phys Chem Chem Phys 7:375–383. https://doi.org/10.1039/b411377b

[85] Maillard F, Peyrelade E, Soldo-Olivier Y, et al (2007) Is carbon-supported Pt-WO_x composite a CO-tolerant material? Electrochim Acta 52:1958–1967. https://doi.org/10.1016/j.electacta.2006.08.024

SUPPLEMENTARY MATERIALS

Synthesis and characterization of graphite oxide derived TiO_2-carbon composites as potential electrocatalyst supports

Ilgar Ayyubov[1], Irina Borbáth[1], Zoltán Pászti[1], Zoltán Sebestyén[1], Judith Mihály[1], Tamás Szabó[2], Erzsébet Illés[2], Attila Domján[3], Mihaela Florea[41], Dana Radu[4], Andrei Kuncser[4], András Tompos[1], Emília Tálas[1]

[1]*Research Centre for Natural Sciences, Institute of Materials and Environmental Chemistry, Eötvös Loránd Research Network (ELKH), Magyar Tudósok körútja 2, H-1117 Budapest, Hungary*

[2]*Department of Physical Chemistry and Materials Science, University of Szeged, H-6720 Szeged, Rerrich Béla tér 1, Hungary*

[3]*Research Centre for Natural Sciences, NMR Research Group, Eötvös Loránd Research Network (ELKH), Magyar Tudósok körútja 2, H-1117 Budapest, Hungary*

[4]*National Institute of Materials Physics, 405A Atomistilor Street, 077125, Magurele, Romania*

[1]corresponding author, Tel.:+40721760041, email: mihaela.florea@chimie.unibuc.ro <mailto:mihaela.florea@chimie.unibuc.ro>, address: National Institute of Materials Physics, 405A Atomistilor Street, 077125, Magurele, Romania (Mihaela Florea))

S1. Experimental

Synthesis of electrocatalyst supports

A transparent acidic TiO_2 colloidal solution was made first by adding Ti(O-*i*-*Pr*)$_4$ into the vigorously stirred mixture of cc. HNO_3 and distilled water. In case of GO derived samples the volumes of H_2O and cc. HNO_3 were calculated to adjust the concentration of Ti(O-i-Pr)$_4$ to 0.115 M and of HNO_3 to 0.69 M in the first step of the procedure (5 h stirring). The suspension with the desired amount of GO was weighted. For exfoliation of it, NaOH solution (pH~ 14) was added to the GO suspension till its pH became ~9. This suspension was sonicated for 25 min. Then the colloidal TiO_2 solution was poured to the GO suspension quickly under vigorous stirring. After that aqueous HNO_3 solution (prepared from 0.4 mL cc. HNO_3 and 7.9 mL H_2O) was added into the slurry. The pH of the slurry was adjusted to that of TiO_2 sol with cc. HNO_3 and the reaction mixture was stirred continuously for 6 days at room temperature (RT) for aging in order to facilitate rutile nuclei formation. After six days of aging, the mixture was centrifuged. The solid part was washed three times with diluted nitric acid in order to remove the well soluble $NaNO_3$. Finally, the solid was re-suspended in diluted HNO_3 of the same volume. After the removal of $NaNO_3$, the slurry was evaporated at 65 °C and dried overnight in an oven at 85 °C.

In case of the solvothermal treatment (ST) step, the solid sample dried at 85 °C was sonicated in 100 mL 2-propanol for a short time (5-10 min) then the slurry was placed into a glass lined autoclave. After rinsing with nitrogen the temperature inside was increased to 140-150 °C in ~1-1.5 h and it was kept at this temperature for ~3 h on autogenic pressure. The reaction mixture was then allowed to cool, centrifuged, air-dried at RT and dried again in an oven at 85 °C overnight.

As a final step of the synthesis of the catalyst support material, a high temperature treatment (HTT) for 8 h at 600 °C in Ar atmosphere was performed to get well crystallized rutile TiO_2.

Synthesis of Pt electrocatalysts

The TiO_2-C support materials were loaded with 20 wt.% Pt via a modified, sodium borohydride ($NaBH_4$) assisted ethylene-glycol (EG) reduction-precipitation method in order to

obtain platinum containing electrocatalyst as we described before [1]. The flow chart of Pt loading process is depicted in Figure S1.

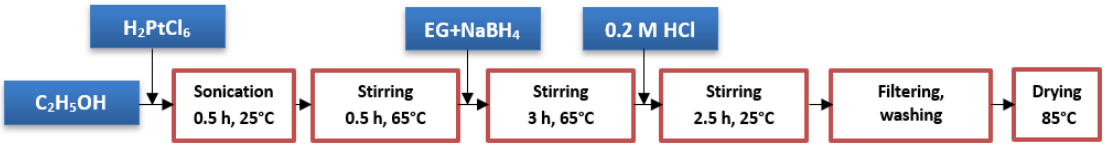

Figure S1. Platinum loading process flow chart

Physical characterization

X-ray powder diffraction (XRD) patterns were obtained in a Philips model PW 3710 based PW 1050 Bragg-Brentano parafocusing goniometer using CuKα radiation (λ= 0.15418 nm), graphite monochromator and proportional counter. Silicon powder (NIST SRM 640) was used as an internal standard and the scans were evaluated with profile fitting methods. The cell parameters of the crystalline phases were determined from the fitted values.

Nitrogen physisorption measurements were carried out at temperature of liquid nitrogen using Thermo Scientific Surfer automatic volumetric adsorption analyzer (Thermo Fischer Scientific, Berlin, Germany). The specific surface area was calculated by the BET method in the range of relative pressures from 0.05 to 0.30.

X-ray photoelectron spectroscopy (XPS) measurements were performed using an electron spectrometer manufactured by OMICRON Nanotechnology GmbH (Germany). MgKα (1253.6 eV) radiation was used as excitation source and data were acquired with 1 eV spectral resolution (30 eV pass energy). The powdered composite supports and catalysts were suspended in isopropanol and drops of this suspension were dried onto stainless steel sample plates. Spectra were processed with the CasaXPS package [2] by fitting the measured data with a combination of Gaussian-Lorentzian product peaks over a Shirley-type background, while quantitative evaluation of the data was performed with the XPSMultiQuant package [3] during which a homogeneous depth distribution was assumed for all components. Chemical states were identified using the NIST database [4], the publication [5] or other literature as indicated. Binding energies were referenced to the lowest binding energy contribution of the C 1s envelope, which was assigned to graphite-like (sp^2-hybridized) carbon in the active carbon backbone (284.4 eV).

ATR-IR spectra were recorded by the means of a Varian 2000 (Scimitar Series) FT-IR spectrometer (Varian Inc, US) equipped with an MCT (Mercury-Cadmium-Telluride) detector and with a 'Golden Gate' diamond single reflection ATR unit (Specac Ltd, UK). 64 scans were collected at a spectral resolution of 4 cm^{-1}. Baseline correction was performed using the GRAMS/AI (7.02) software (ThermoGalactic Inc., US).

Solid state NMR magic angle spinning (MAS) spectra of samples were recorded on Varian System spectrometer with a Chemagnetics 3.2 mm narrow-bore triple resonance T3 probe in double resonance mode. The spinning rate of the rotor was 10 kHz for the ^{1}H, ^{13}C measurements. For direct polarization ^{13}C spectra 15000 transients were recorded with SPINAL-64 decoupling and 20 s of relaxation delay. The measuring temperature was 20 °C. Adamantane was used as external chemical shift reference (38.55 and 29.50 ppm). The 90° pulse lengths were 2.9 μs for carbon and 2.9 μs for the proton channel.

Transmission Electron Microscopy (TEM) studies of the samples were made by use of a JEOL 3010 high resolution transmission electron microscope operating at 300 kV. The structure has been identified by Selected Area Electron Diffraction (SAED) and the compositional homogeneity has been checked by Scanning Transmission Electron Microscopy (STEM) coupled with Energy Dispersive X-Ray Spectroscopy (EDS). The samples for TEM analysis were prepared by dripping on a microscopy grid, deposited initially on a carbon membrane, a few drops from the material suspension obtained by immersion of the powder in ethanol.

Scanning electron micrographs of the samples were recorded with a scanning electron microscope Vega II LMU model from Tescan, equipped with an energy dispersive X-ray spectrometer (EDX) Bruker Quantax 200, at the following operational parameters: accelerating voltage 30 kV, measuring time 1200 s, working distance around 17 mm, counting rate 0.4 kcps.

Thermogravimetric (TG) measurement was carried out with a PerkinElmer TGS-2 thermoscale in a compressed air atmosphere. The flow rate (volumetric flow) of the gas was 140 ml/min during the test. Approx. 1 mg sample was weighed. The TG furnace heat program has heated the sample from room temperature (1-minute running time) to 900 °C.

Electrochemical characterization

A Biologic SP 150 potentiostat and a standard three-electrode electrochemical cell were used for the electrochemical measurements. The applied electrolyte was 0.5 M H_2SO_4 solution, which was prepared by using Milli-Q water and concentrated H_2SO_4.

Glassy carbon (GC; d= 0.3 cm) electrode with 0.0707 cm^2 surface area was used as working electrode. Platinum wire was used as counter electrode and a hydrogen electrode as reference electrode. All potentials are given on RHE scale. The details of the working electrode preparation, the catalyst ink composition and electrocatalytic measurements were described in Refs. [6, 7].The Pt loading of the electrodes was 10 μg cm^{-2}.

Electrocatalytic performance of the 20 wt.% Pt/TiO_2-C electrocatalysts was studied by cyclic voltammetry and CO_{ads}-stripping voltammetry measurements combined with stability test involving 500 polarization cycles and the second CO_{ads}-stripping voltammetry measurement. In the long-term stability test, the samples were submitted to cyclic polarization at 100 mV s^{-1} scan rate for 10,000 cycles between 50 and 1000 mV potential limits; these measurements took ca. 54 hours.

The charges associated with hydrogen underpotential deposition, $Q_{ox_{Hupd}}$, were calculated using conventional baseline correction. From the oxidation charge of the monolayer hydrogen the electrochemically active Pt surface area ($ECSA_{Hupd}$) can be calculated using the Equation 1 [8]:

$$ECSA_{Hupd}\ (cm^2) = Q_{ox_{Hupd}}\ (\mu C) / 210\ (\mu C/cm^2) \qquad \text{(Equation S1)}$$

where $ECSA_{Hupd}$ is the electrochemical surface area determined from the amount of underpotentially deposited hydrogen on the platinum surface; $Q_{ox_{Hupd}}$ is the oxidation charge of underpotentially deposited hydrogen obtained from the CV experiment and 210 (μC/cm^2) is the amount of charge required to oxidize monolayer hydrogen adsorbed on 1 cm^2 of polycrystalline platinum surface.

Results concerning on the change of the electrochemically active Pt surface area upon the N-cycle stability test are presented as $ECSA_N$ (N: 500, 2,500, 5,000 and 10,000) normalized to $ECSA_1$ measured in the first cycle on the same sample. Another measure of the change of the electrochemically active Pt surface area is the ΔECSA value defined in Equation 2 [9]:

$$\Delta ECSA_N = \{1-(ECSA_N/ECSA_1)\}\times 100\% \qquad \text{(Equation S2)}$$

After every stability test the electrolyte was changed to fresh one to avoid the re-deposition of the dissolved metals.

Catalytic activity of the catalyst samples was tested in the ORR by rotating disc electrode (RDE) technique. The ORR measurements were done in O_2 saturated 0.5 M H_2SO_4 solution at ambient temperature and pressure. Polarization curves were recorded by sweeping the potential between 300 and 1000 mV with 10 mVs^{-1} sweep rate, rotating the electrode at six rotation speeds (225, 400, 625, 900, 1225 and 1600 revolutions/min (rpm)). Data were obtained

from the negative scans. In this study activities in the ORR (current densities) were expressed as current values normalized to the geometric surface area of the electrode.

ORR measurements combined with 500-cycle stability test and the second ORR measurements were also performed.

S.2 Physicochemical characterization

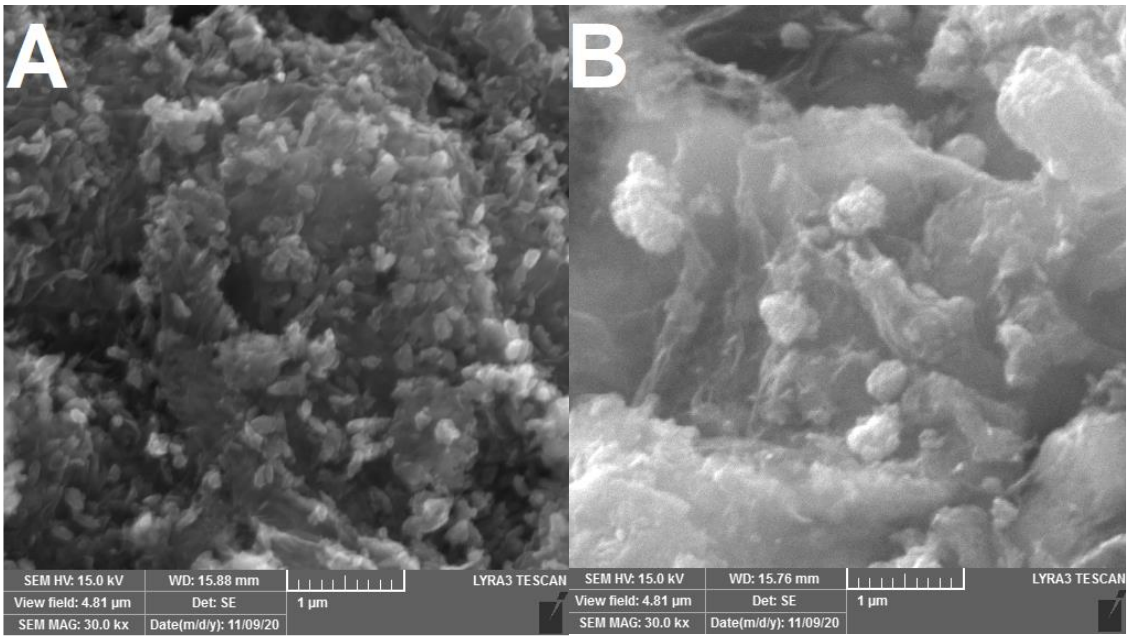

Figure S2. SEM images of TiGO-1 derived samples after various treatments.
A: TiGO-1; B: TiGO-1ST.

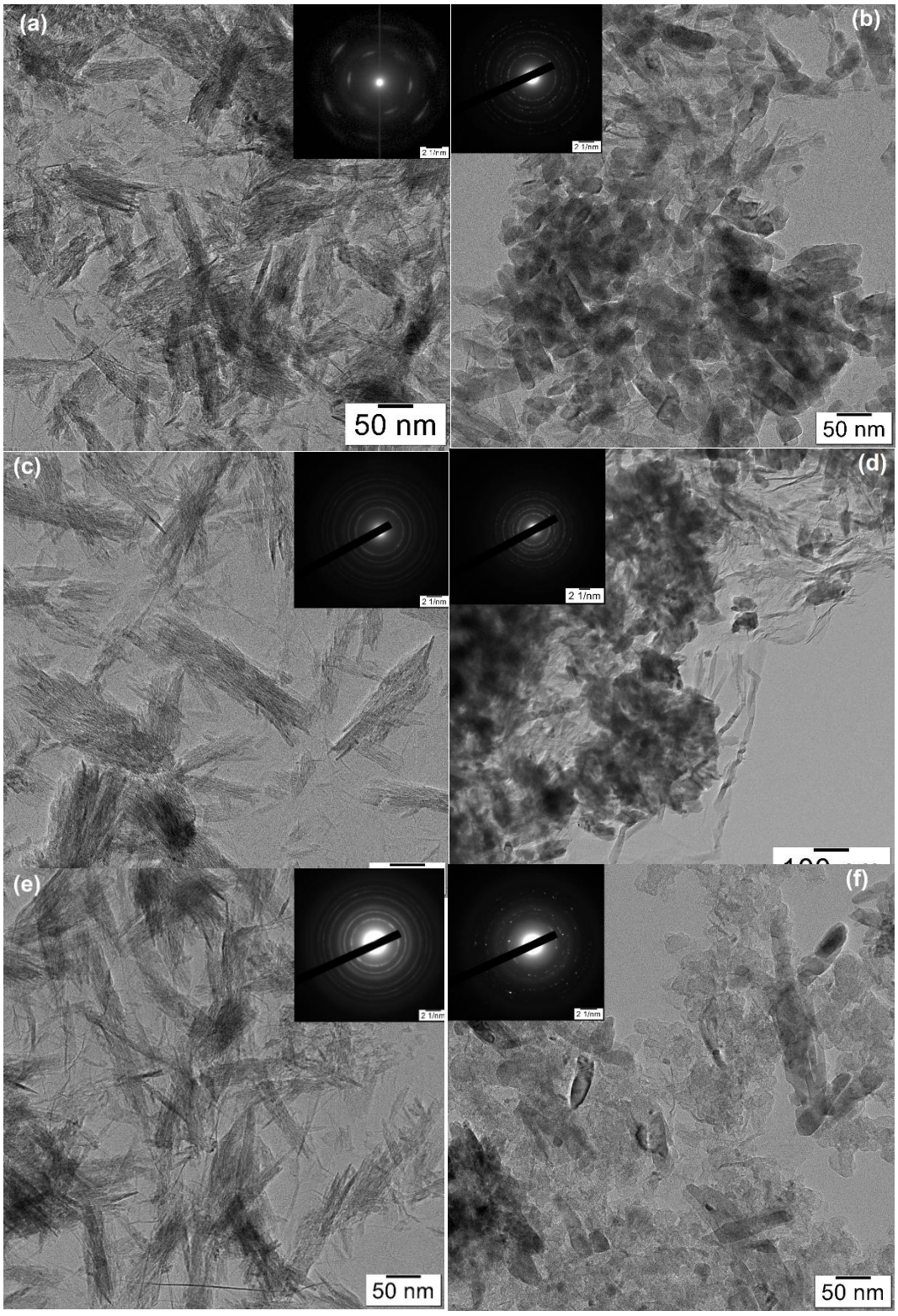

Figure S3. TEM images of TiGO-1 (a),TiGO-1HT(b), TiGO-2 (c), TiGO-2HT (d), TiGO-3 (e), TiGO-3HT (f).

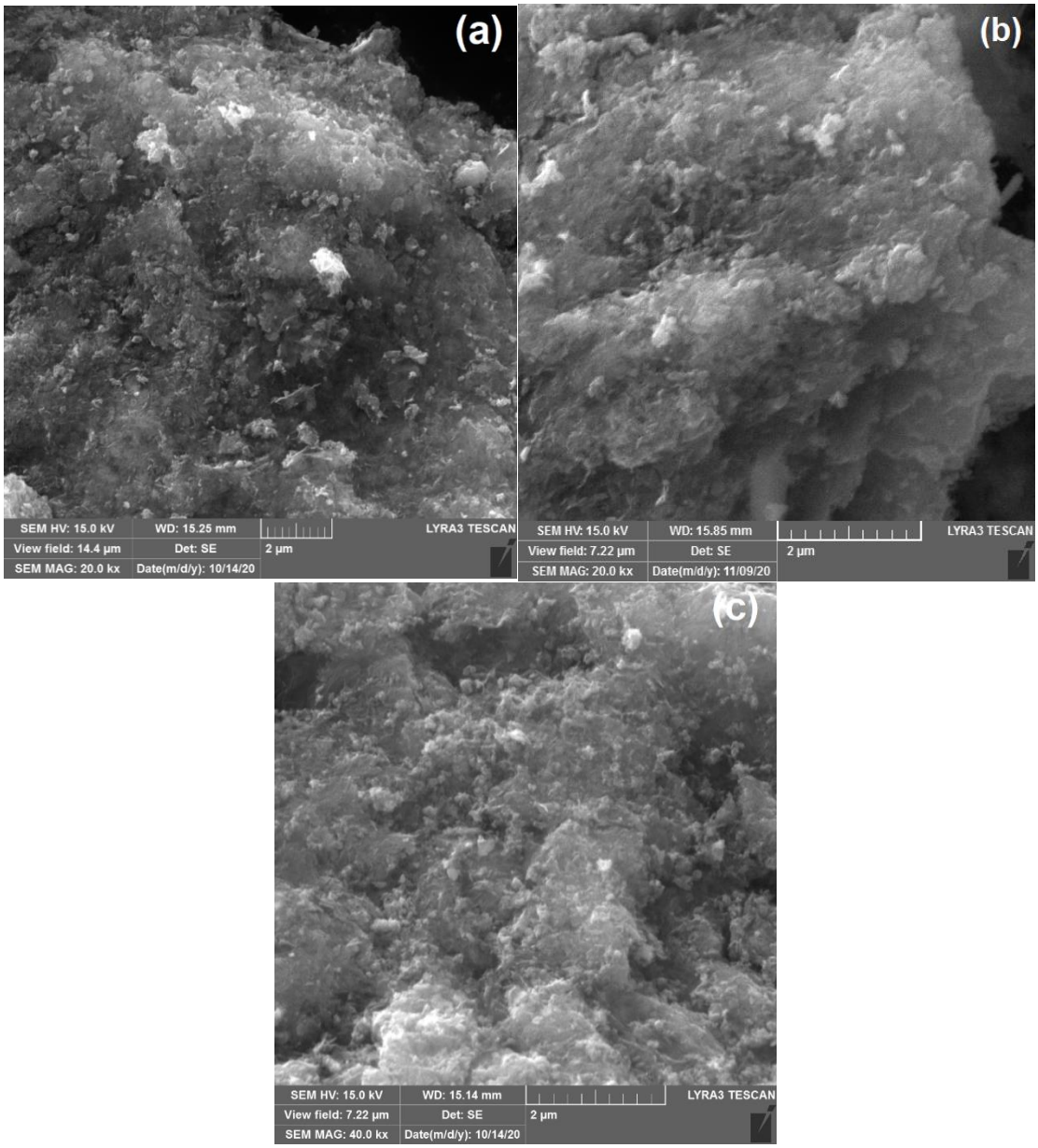

Figure S4. SEM images of (a) TiGO-1HT, (b) TiGO-2HT and (c) TiGO-3HT samples.

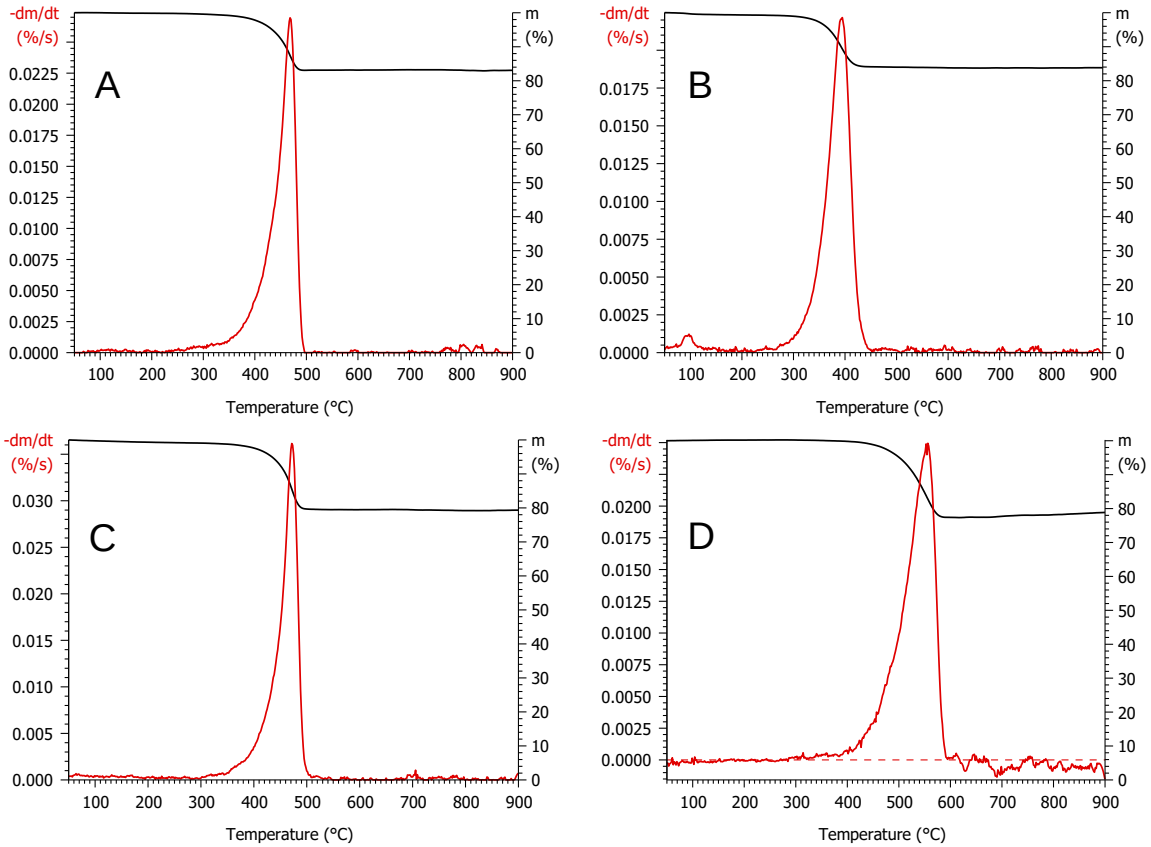

Figure S5. TG and DTG patterns of TiO_2/carbonaceous material composite type of samples. A: TiGO-1HT (carbonaceous part derived from GO(I) without additional washing step), B: TiGO-2HT (carbonaceous part derived from GO(II) without additional washing step), C: TiGO-3HT (carbonaceous part derived from GO(II) with additional washing step), D: TiBPHT (carbonaceous part derived from Black Pearls 2000 (BP) carbon).

Table S1. Results of nitrogen physisorption measurements of TiO_2-C samples (see denomination of the samples and details of their preparation in Table 1 in the main document)

Sample	Surface area (m^2/g)	Mesopores surface area (m^2/g)	Total pore volume (cm^3/g)	Micropore volume (cm^3/g)	Maximum pore diameter (nm)
TiBPHT	300	n.r.	0.60	0.15	0.16
TiGO-3HT	264	236	0.69	0.03	n.r.
TiGO-1STHT	198	198	0.46	0.01	n.r.
Parent BP [10]	1635	n.d.	n.d.	0.59	n.d.
[11]	1485	n.d.	n.d.	n.d.	n.d.

n.d.: no data;
n.r.: not relevant

In case of the BP derived TiO_2-C (TiBPHT) sample, the shape of the isotherm (see Fig. 8B in the main document) indicated that mesopores were not characteristic for this composite, however certain amount of micropores were present. Pore size distribution curve of sample TiBPHT are shown in Figure S6. According to Figure S6 the maximum pore diameter was 0.16 nm. The difference of the total pore volume and micropore volume could be attributed to the macropore volume or the volume between the particles.

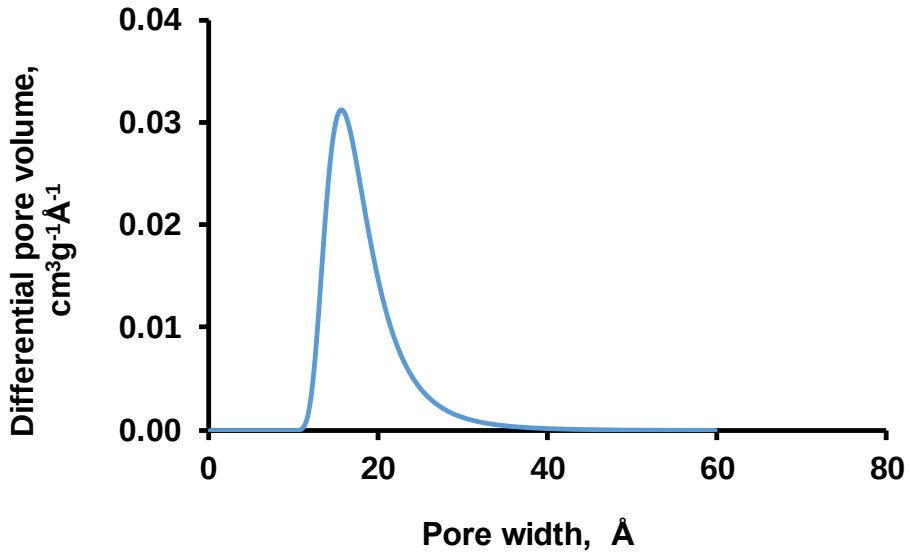

Figure S6. Pore size distribution of the BP derived TiO_2-C (TiBPHT)

In case of sample TiGO-3HT (see Fig. 8A in the main document) the H3 loop appeared, therefore pore size distribution cannot be obtained according to Ref. [12]. Sample TiGO-1STHT showed also H3 loop.

S.3 Electrochemical characterization

The results of the electrochemical characterization of the TiO_2-C composite supported 20 wt.% Pt catalysts studied by cyclic voltammetry and CO_{ads}-stripping voltammetry measurements done before and after the 500-cycle stability test, as well as by the long-term stability test involving 10,000 polarization cycles were presented in Table S2. For comparison, the results of the study of the 20 wt.% Pt/ $Ti_{0.8}Mo_{0.2}O_2$-C (C= BP and GO derived) catalysts and commercial 20 wt.% Pt/C (Quintech) presented in Ref. [9] were also included.

Table S2. Electrochemical characterization of the TiO_2-C and the $Ti_{0.8}Mo_{0.2}O_2$-C composite supported 20 wt.% Pt catalysts. Effect of the presence of molybdenum.

Sample	**$E_{CO,max}$,** [a] **mV**	**$ECSA_1$, m^2/g_{Pt}**	**$\Delta ECSA_{500}$, % [b]**	**$\Delta ECSA_{10,000}$, % [b]**
Pt/75TiO_2-25GO	775 (sh: 705)	82.9	6.4	34.3
Pt/75$Ti_{0.8}Mo_{0.2}O_2$-25GO [c]	705 (*sh:* 745)	77.6	8.4	36.0
Pt/75TiO_2-25BP	775 (sh: 705)	82.0	7.0	39.9
Pt/75$Ti_{0.8}Mo_{0.2}O_2$-25BP [c]	705 (*sh:* 745)	81.6	7.4	37.0
Pt/25$Ti_{0.8}Mo_{0.2}O_2$-75BP [c]	775	69.1	11.8	27.6
Pt/C [c]	795	94.5	12.7	47.8

[a] The position of the main CO stripping peak and shoulder in brackets (***sh***) obtained on fresh catalysts;

[b] $\Delta ECSA_{500}$ and $\Delta ECSA_{10,000}$ were calculated according to the Equation S2;

[c] From Ref. [9].

As can be seen from Table S2, the addition of Mo to composites obtained using carbonaceous materials of a certain type and the same oxide/carbon ratio does not affect the ECSA and the stability of the related Pt electrocatalysts.

Nevertheless, it is obvious that the presence of molybdenum in the catalyst increases the CO tolerance to a significant extent. Thus, the position of the main CO_{ads} stripping peak (705 mV) on the Mo-containing Pt/$Ti_{0.8}Mo_{0.2}O_2$-C catalysts with 75 weight% of mixed oxide in composite was shifted towards less positive potentials by 70 mV with respect to the main peak observed on the Mo-free samples (775 mV). Moreover, according to our previous studies [9, 13], in contrast to the Mo-free samples, on Mo-containing catalysts the electrooxidation of CO (the so-called “pre-peak”) started at exceptionally low potential values ($E_{CO,onset}$= 50 mV).

As shown in Table S2 decrease of the mixed oxide content in composite materials ($Ti_{0.8}Mo_{0.2}O_2$/C= 25/75) results in a shift of the main CO_{ads} stripping peak in the direction of more positive potentials (775 mV), which may be due to a decrease of Pt sites, where Pt and atoms of oxophilic metal/metals (Mo, Ti) are in atomic closeness.

In this respect, the results obtained on the Pt/TiO_2-C catalysts with a nominal TiO_2/C= 75/25 ratio are rather unexpected. However, an explanation for this phenomenon can be found taking into account the results of XPS and TEM, suggesting significant sintering of titania in Mo-free catalysts during high-temperature treatment leading to the formation of relatively large crystallites with incomplete coverage of the carbon backbone.

References

[1] Vass Á, Borbáth I, Pászti Z, et al (2017) Effect of Mo incorporation on the electrocatalytic performance of Ti–Mo mixed oxide–carbon composite supported Pt electrocatalysts. React Kinet Mech Catal 121:141–160. https://doi.org/10.1007/s11144-017-1155-5

[2] Fairely N (2009) CasaXPS Manual 2.3. 15. Casa Softw Ltd 1–177

[3] Mohai M (2004) XPS MultiQuant: Multimodel XPS quantification software. Surf Interface Anal 36:828–832. https://doi.org/10.1002/sia.1775

[4] Wagner CD, Naumkin A V., Kraut-Vass A, et al (2003) NIST X-ray photoelectron spectroscopy database

[5] Moulder J, Stickle W, Sobol P, Bomben K (1981) Handbook of X-ray Photoelectron Spectroscopy Perkin-Elmer Corp., Physical Electronics Division, Eden Prairie, Minnesota, USA, 1979.

[6] Vass Á, Borbáth I, Bakos I, et al (2019) Stability issues of CO tolerant Pt-based electrocatalysts for polymer electrolyte membrane fuel cells: comparison of Pt/$Ti_{0.8}Mo_{0.2}O_2$-C with PtRu/C. React Kinet Mech Catal 126:679–699. https://doi.org/10.1007/s11144-018-1512-z

[7] Vass Á, Borbáth I, Bakos I, et al (2018) Novel Pt Electrocatalysts: Multifunctional Composite Supports for Enhanced Corrosion Resistance and Improved CO Tolerance. Top Catal 61:1300–1312. https://doi.org/10.1007/s11244-018-0988-0

[8] Bard AJ (1976) Electroanalytical chemistry : a series of advances. Volume 9. M. Dekker, New York; Basel

[9] Borbáth I, Tálas E, Pászti Z, et al (2021) Investigation of Ti-Mo mixed oxide-carbon composite supported Pt electrocatalysts: Effect of the type of carbonaceous materials. Appl Catal A Gen 620:118155. https://doi.org/10.1016/j.apcata.2021.118155

[10] Pantea D, Darmstadt H, Kaliaguine S, et al (2003) Electrical conductivity of conductive carbon blacks: Influence of surface chemistry and topology. Appl Surf Sci 217:181–193. https://doi.org/10.1016/S0169-4332(03)00550-6

[11] M. Carmo, A.R. dos Santos, J.G.R. Poco, M. Linardi, Physical and electrochemical evaluation of commercial carbon black as electrocatalysts supports for DMFC applications, J. Power Sources 173 (2007) 860–866. https://doi.org/10.1016/j.jpowsour.2007.08.032

[12] F. Rouquerol, J. Rouquerol, K.S.W. Sing, P. Llewellyn, G. Maurin, Adsorption by Powders and Porous Solids. Principles, Methology and Application. (2nd edition) Academic Press, Amsterdam, Boston, Heidelberg, London,New York, Oxford, Paris, San Diego, San Francisco, Sydney, Tokyo , 2012. pp 298.

[13] Borbáth I, Zelenka K, Vass Á, et al (2021) CO tolerant Pt electrocatalysts for PEM fuel cells with enhanced stability against electrocorrosion. Int J Hydrogen Energy 46:13534–13547. https://doi.org/10.1016/j.ijhydene.2020.08.002